

63p.

DEVELOPMENT OF IMPROVED
SINGLE CRYSTAL GALLIUM
PHOSPHIDE SOLAR CELLS

N64 13935

CODE-1

CB-55311

Quarterly Report No. 2

12 September - 12 December, 1963

Contract No. NAS3-2776

Placed by

NATIONAL AERONAUTICS AND SPACE ADMINISTRATION

Lewis Research Center

Cleveland, Ohio

OTS PRICE

XEROX

\$

6.60 ph.

MICROFILM

\$

2.09 mf.

MONSANTO RESEARCH CORPORATION

A SUBSIDIARY OF MONSANTO CHEMICAL COMPANY



DAYTON

LABORATORY

DAYTON 7, OHIO

Requests for copies of this report should be referred to:

National Aeronautics and Space Administration
Office of Scientific and Technical Information
Washington, D. C. 20546
Attn: AFSS-A

NOTICE

This report was prepared as an account of Government-sponsored work. Neither the United States nor the National Aeronautics and Space Administration (NASA), nor any person acting on behalf of NASA:

A). Makes any warranty or representation expressed or implied with respect to the accuracy, completeness, or usefulness of the information contained in this report or that the use of any information apparatus, method, or process disclosed in this report may not infringe privately-owned rights; or

B). Assumes any liabilities with respect to the use of, or for damages resulting from the use of any information apparatus method or process disclosed in this report.

As used above, "person acting on behalf of NASA" includes any employee or contractor of NASA or employee of such contractor, to the extent that such employee or contractor of NASA, or employees of such contractor prepares, disseminates, or provides access to, any information pursuant to his employment or contract with NASA, or his employment with such contractor.

1
DEVELOPMENT OF IMPROVED
SINGLE CRYSTAL GALLIUM
PHOSPHIDE SOLAR CELLS

②
Quarterly Report No. 2,
✓ September 12, 1963 to December 12, 1963

(NASA Contract No. NAS3-2776)

NATIONAL AERONAUTICS AND SPACE ADMINISTRATION

Technical Management
Space Power Systems Division
NASA - Lewis Research Center
Attention: Clifford K. Swartz

[1963] 63p ref

Report Prepared by: ^{d.a.} W. O. Groves and A. S. Epstein

Edited by: R. A. Ruehrwein

Work Performed by:

[7]
c.a. → ^② Central Research Department
MONSANTO CHEMICAL COMPANY
St. Louis, Missouri

5910005

(NASA CR-55311)
OTS: \$6.60 ph,
\$2.09 ref

TABLE OF CONTENTS

	<u>Page Number</u>
I. PURPOSE	1
II. ABSTRACT	2
III. MATERIAL PREPARATION	3
A. Growth Rate	3
B. Structure	6
C. Doping	9
D. Purity	11
E. Conclusions	14
IV. SOLAR CELL FABRICATION	15
V. SOLAR CELL EVALUATION	17
A. Bump Density	18
B. Spectral Response Measurements	18
C. Photo Response of Top Metal Contact to GaP Solar Cell	19
D. Effect of GaP-GaAs Interface	19
E. Solar Cell Characteristics as Function of Temperature	20
F. Diffusion Length Measurements	21
G. I-V Characteristics	22
H. Capacity-Voltage Measurements	23
J. Effect of Junction Depth on Solar Cell Characteristics	24
VI. DISCUSSION	
A. Open Circuit Voltage	25
B. Short Circuit Current Density	25
VII. FUTURE STUDIES	27
VIII. REFERENCES	29
APPENDIX A	30
APPENDIX B	31

I. PURPOSE

This report presents the work done during the second quarter of the Single Crystal Gallium Phosphide Solar Cell program. The objective of this program is the development of an efficient solar cell operable at temperatures up to 500° C. The approach is to grow single crystal gallium phosphide by epitaxial deposition from the vapor phase on gallium arsenide substrate followed by removal of the gallium arsenide. Diffused junction cells are then fabricated and the photovoltaic properties of the cells are measured, ultimately up to 500° C. The design and performance of the cells are to be related to the electrical and optical properties of the gallium phosphide.

II. ABSTRACT

13935

Single crystal gallium phosphide has been prepared by epitaxial deposition on single crystal gallium arsenide using hydrogen chloride in an open tube vapor transport process with excess phosphorus and either gallium or gallium phosphide sources. The growth rate in this system depends in a complex way on gas flow rates, on substrate position and temperature, and on total substrate area. Structural perfection depends on three interdependent factors, surface orientation, surface preparation and run conditions, the latter including impurity composition of the gases. Doping with tellurium and zinc has been demonstrated. The gallium phosphide, as indicated by electrical measurements, has been highly compensated, with several different, as yet unidentified, impurities being implicated.

Solar cell characteristics measured at room temperature have generally fallen into two categories: (1) high open circuit voltage and low short circuit current densities, (2) low open circuit voltages and high short circuit currents. In the former group of cells an open circuit voltage of 1.18 volts has been achieved with a short circuit current density of $\sim 0.1 \text{ ma/cm}^2$. In the latter category cells having a short circuit current density as high as 5 ma/cm^2 have been obtained with open circuit voltages around 0.7 volts. These cells have their main spectral response at wavelengths of the order of 0.7μ whereas cells of category (1) respond more to the band edge absorption.

One cell at room temperature when measured with a tungsten source had a conversion efficiency of 2.5%. This cell came from the second category.

With increase in temperature the short circuit current generally tends to increase whereas the open circuit voltage decreases. *Author*

III. MATERIAL PREPARATION

The open tube, HCl transport process for growing GaP layers epitaxially on GaAs substrates and the techniques for measuring their electrical properties have been described in Quarterly Report No. 1.

Continuing from the first quarter, the principal effort during this period has been on defining factors affecting growth rate, and on conditions causing formation of bumps and other defects. In addition, preliminary experiments have been made on control of net carrier level by doping. Some efforts to improve purity have also been initiated.

A. Growth Rate

A principal objective of the materials preparation has been to grow thick self-supporting layers of GaP in order that solar cell properties may be studied free from possible interfering effects from a GaAs substrate. Progress toward this goal has been slow but a number of factors affecting growth rate have been elucidated in the process of other investigations and the goal now appears within reach.

Some thick epitaxial wafers have been grown in closed tube experiments (on a separate company-funded program). The structure of these wafers, grown in the $\langle 111 \rangle$ A direction, is rather poor and the characteristics of a solar cell fabricated from one are also poor (sample CTVIII, Table V). At present, no advantage can be seen in the closed tube process.

Run conditions and resulting growth rates are summarized in Table I for all runs made this period in the open tube system. The runs are tabulated in order of increasing growth rate. Similar data for earlier runs are given in Table I of Quarterly Report No. 1. All runs were made using the pretreatment in phosphorus vapor at 1000° C described in that report.

The source material, gallium or gallium phosphide, and dopant, either vaporized separately or dissolved in the source gallium, are indicated in column 2, approximate source temperature in column 3.

The position of the substrate wafer in the furnace, column 4, may be compared with the "dump zone" centered at 13-1/2". Approximate substrate temperatures are listed in column 5.

Hydrogen flow rates are from flow meter readings. The HCl flow rates are derived from the weight loss of the Ga or GaP source. For comparison, the actual HCl flow rates based on a calibration of the flow meter are given in parenthesis for Runs SC25 on. The phosphorus flow rates are averages calculated from total weight loss, including that during the pretreatment period, except for runs SC25 and SC26. In these runs the flow rate was reduced from the initial high rate to the low rate indicated after initiation of deposition. Actual rates during the pretreatment are higher and during deposition are lower than the averages given. For example, in a typical run averaging 1.2 cc/min after 240 minutes the flow rate will have fallen to about 0.4 cc/min.

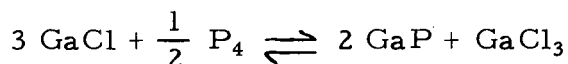
Duration of deposition period, approximate layer thickness (derived from measurements on Hall bars), and average growth rates are given in columns 9 through 11. In the last column growth rates have been divided by HCl flow rates to yield the average growth rate in microns per cc of HCl.

Under the conditions given, growth rates are seen to vary by nearly a factor of ten from 0.04 to 0.38 μ /min. The range is reduced somewhat if the normalized growth rate, in μ /cc HCl, is considered since it appears that for H_2/HCl ratios greater than 150 the growth rate is proportional to HCl flow rate.

The low growth rate in SC21 may have been due principally to the high rate of back diffusion and convection at this very low total flow rate. This could have allowed transport of material from the wafers to cooler regions downstream and would account for the etching and very ragged interface observed. However, the low H_2/HCl ratio may also have been a contributing factor to the low growth rate (see

SC6 and SC7 in Table I of Quarterly Report No. 1).

The low growth rates obtained in runs SC25 and SC26 must be attributed to the low phosphorus pressure. Although masked by other factors, a trend toward higher growth rates with increasing phosphorus pressure may also be seen in the remaining runs. This can be expected from the effect of phosphorus pressure on the equilibrium of the deposition reaction,



The effect of the position of the substrate in the furnace may best be seen in the results from runs in which two wafers were included (SC18, SC19, and SC24). The effect of moving the wafer upstream into the "dump" zone is not as pronounced however, as the data in the first quarterly report would indicate. The effect will depend on both substrate temperature and temperature gradient, both of which decrease in this region. Further advance of the substrate into a zone of higher temperature reduces the growth rate.

The growth rate depends on the area available for deposition and is generally lower as the number or size of the wafers is increased. It will also decrease as a deposit builds up on the wall to provide a competing deposition site. Therefore the growth rate decreases with time. This effect is masked by the effect of phosphorus pressure in these data.

Doping does not appreciably affect growth rate except at very high levels where growth habit of the bump structure is radically changed (SC16) as will be shown later or the number of bumps is increased to the point that overlapping occurs. A high concentration of overlapping bumps will increase the average layer thickness and hence the apparent growth rate.

In the several runs in which a higher source temperature was used, the wafers were located farther downstream so as to leave the gradient at the wafer position essentially unchanged and no appreciable affect on

growth rate is observable.

Another factor which might account for some variation in the growth rates and the generally low rates is the position of the substrate in the tube relative to the vertical temperature distribution in the split tube furnace. Normally, the wafers are supported on a quartz plate 4 to 5 mm below the tube center. In two runs, SC27 and SC28, the wafers were supported vertically (still parallel to the flow direction) to take advantage of the lower temperature opposite the hinged opening of the furnace. While a reduction of deposit on the tube wall was noted, competition between growth on the front and on the back of the wafer kept the growth rates low. Furthermore, the layer had poor uniformity of thickness. In Run SC30 the wafer was supported horizontally in the center of the tube on a thicker quartz plate. The above average growth rate (in μ / cc HCl) relative to the very limited deposit on the wall near the wafers is very encouraging although the other run conditions were less than ideal.

A final factor which may affect growth rate is the precise orientation of the wafer surface relative to the $\langle 100 \rangle$ plane. No experiments have been done but the possibility is suggested by the growth habits of bumps as discussed in the next section.

B. Structure

"Stacking faults" and other structural defects associated with bumps on the surface of epitaxially grown wafers in extreme cases lead to non-planar junctions on diffusion (Fig. 19, Quarterly Report No. 1). While the incidence and severity of these defects is greatly reduced by a high temperature phosphorus pretreatment of the substrate as described in the first quarterly report they are not completely eliminated. Although at present no significant effect on solar cell properties can be attributed to the remaining bumps, a deleterious effect may be uncovered at some later stage in the development when other current limitations have been removed. For this reason, and because bumps may be associated with

or indicate the presence of other undesirable elements, it is worthwhile to try to understand the conditions under which they are formed.

Three interdependent factors appear to be involved in the formation of bumps: surface preparation; surface orientation; and growth conditions. Surface preparation is critical. The origin of most bumps can be traced to the epitaxial-substrate interface where they have been nucleated by dirt or damage on the surface.

At present, no cleaning technique produces perfectly clean surfaces although some improvement has been made. The present technique consists of cleaning the polished and dewaxed wafers ultrasonically in concentrated H_2SO_4 followed by rinsing in distilled water and ethyl alcohol. On removal from the alcohol the wafers are wiped dry with microcloth and immediately loaded into the reactor. For one run, SC24, one of the wafers was simply lapped, etched in a polish etch, rinsed in deionized distilled water and dried in a nitrogen jet. The resulting surface was streaked with haze but the bump structure did not correlate with this haze and was equivalent to that of the standard wafer.

Surface orientation has recently been recognized as a major factor in the formation of bumps, and is the primary if not the only cause of the differences observed for different substrates in the same run. The more closely the surface approaches exact $\langle 100 \rangle$ orientation the more critical do the surface preparation and run conditions become. If the surface is slightly off orientation the growth mechanism apparently permits potential or actual bump sites to be overridden and buried. Perfectly oriented surfaces become covered with incipient bumps, many of which develop into full blown bumps which may then engulf less active neighbors. A systematic study of the effect has not yet been made. Neither has an attempt yet been made to obtain wafers deliberately cut and polished off orientation. On the other hand, the availability of a set of nearly perfectly oriented wafers has increased the sensitivity of the growth experiments to the other factors causing bumps.

A deposit nearly free of bumps is shown in Figure 1. The orientation effect here is evident. A high concentration of bumps appears near the lower edge where the surface was "on orientation" due to slight curvature introduced by polishing. The few isolated bumps (of the "square pyramidal" type) appear to be tipped over with one edge partially buried in the surface. The line at the lower edge was caused by the support holding the wafer in a vertical position.

The growth conditions affecting bump formation include flow rates of H_2 , HCl and phosphorus, temperature and temperature gradient at the substrate positions, or, in short, all the conditions discussed above in connection with growth rate. The most striking effect is that of impurity dopants on the growth habits of the bumps. This is illustrated in Figures 2, (a), (b), (c) and (d) and 3, (a), (b), (c) and (d). In earlier "undoped" runs (Figure 2 (a) and Figures 8 and 9 of Quarterly Report No. 1) the bumps tended toward a rounded rectangular base shape with axes in $\langle 110 \rangle$ directions, frequently with a flattened top. Moderate doping with tellurium produces bumps of the same shape, but very heavy doping with tellurium draws the bumps out into long parallel ridges (Figure 2 (c)). Recent "undoped" runs have produced bumps having the "square pyramidal" configuration illustrated in Figure 1 (b). Doping with Zn elongates the bumps in the other $\langle 110 \rangle$ direction (Figure 1 (d)).

Details at the peaks of some typical bumps are shown in Figure 3 (a), (b), (c) and (d). One feature all have in common is the lack of symmetry expected for a $\langle 100 \rangle$ oriented structure. If we label the slopes of the bumps, A and B, (as for the sides of a pyramid formed by $\langle 111 \rangle$ faces on a $\langle 100 \rangle$ base) the Te doped bumps are elongated in the B direction, the Zn doped bumps in the A direction. The peak of the bump in each case is symmetrical with the B slopes but displaced in one or the other of the A directions. Displacement in the B direction has never been observed.

The square arrays in Figures 3 (a) and (c) are believed to be stacking faults in the $\langle 111 \rangle$ planes intersecting the surface. The size of the square corresponds with the base of a pyramid formed by $\langle 111 \rangle$ planes with its apex at the GaP-GaAs interface. An example of a very high concentration of these "stacking faults" in a cleaved section was shown in Figure 19 of Quarterly Report No. 1.

The other short "hash marks" on the B slopes of the bumps in Figures 2 (a), (b), (c) and (d) are small growth steps. These steps also appear in smooth bump free areas of the wafers (Figure 14, Quarterly Report No. 1), but are strong only if the surface is tipped in the B direction with respect to the $\langle 100 \rangle$ planes.

Impurities added through the vapor phase other than intentional dopants may also affect the structure. In some runs many bumps have had holes, or polycrystalline material at the peaks. In run SC-5 (Figure 12 Quarterly Report No. 1) this has been attributed to the oxygen impurities in the impure phosphorus. There is some indication that a high phosphorus pressure reduces the growth of the bumps in height and produces the flat topped bumps. This effect may be direct or indirect through influence on the distribution of impurities.

Finally a disturbance in the run such as a sudden pressure drop may induce bump formation after smooth growth has been initiated. This is believed to be the cause of the poor surface of SC10-2 (Figure 10, Quarterly Report No. 1) and the bumps on SC30-3 (Figure 2(d)). These latter bumps are about one half the size expected for the thickness of the layer and were probably all nucleated at a point midway in the run when a pressure buildup due to plugging of the exit tube was relieved.

C. Doping

The net carrier level of "undoped" epitaxial GaP layers ranges up to the mid- 10^{17} cm^{-3} range, n-type (Table II and Table II of Quarterly Report No. 1). This level will hopefully be reduced as purer material

is developed. Therefore, to control the net carrier level in the range up to 10^{19} cm^{-3} n-type, or to produce p-type material, impurity dopants must be added deliberately.

Doping with tellurium and zinc has been accomplished by vaporizing the elements into the H_2 -HCl stream from a boat in the first furnace. In the case of tellurium, as will be shown later, almost all of the dopant dissolved in a liquid gallium source. This doped source also was subsequently used to produce heavily n-type epitaxial layers. In the case of zinc, not enough dopant remained in the source to form p-type deposits on reuse, but the zinc did influence the growth habit of the bumps (Figure 3 (d)).

Data on electrical properties of these doped samples are summarized in Table III. The conditions under which they were made may be found in Table I. For runs SC16, SC18 and SC19, under source, the rate of evaporation of tellurium in atoms/unit time based on total weight loss is expressed relative to the rate of consumption of source in cc of solid GaP equivalent per unit time. Thus the expressed doping rate is equivalent to that from a GaP source doped to the same level. In run SC16, using a GaP source, the carrier level of the epitaxial layer is of the same order of magnitude as that of the "source". The results from SC18 are ambiguous because the epitaxial carrier level is only slightly higher than the normal undoped level, but in SC19 the epitaxial carrier level is a factor of twenty less than the "source" level. This is a good indication that the gallium source has dissolved most of the tellurium passing over it. Solution of all of the tellurium would have produced a concentration equivalent to $2.3 \times 10^{18} \text{ cm}^{-3}$ in the original source. Subsequent use of this source did, indeed, produce increasingly doped epitaxial layers as shown by the series SC20 through SC23, and confirms the high solubility of tellurium in gallium. This tendency of the dopant to concentrate in the source will add an additional complication to accurate control of doping.

Comparable results are indicated by two zinc doping runs in one of which zinc was vaporized separately. The zinc weight loss was not obtained, but the approximate temperature is indicated. The results suggest that only a fraction of the zinc in the vapor phase is incorporated in the epitaxial deposit. Thus, in SC30 the doping was insufficient for conversion to p-type although, as noted above, the bump habit was affected.

D. Purity

The purity of the material, because of its effect on lifetime, is probably the most critical factor affecting the properties of a gallium phosphide solar cell. The "undoped" epitaxial gallium phosphide produced to date, besides having a high net carrier level, is highly compensated as indicated by low mobilities. The data are listed in Table II. Although no systematic attempt to identify the nature and source of the principal impurities has yet been attempted, the following observations relative to purity have been made.

The electrical properties of the epitaxial layer may be independent of the phosphorus source used. The phosphorus source used through run SC16 was of "five 9's" purity with the exception of an ordinary laboratory grade employed in run SC5. That used for run SC17 on was a granular "semiconductor" grade in which approximately 0.001% each of Mg, Al, Si and Fe have been detected spectroscopically, the Cu content not determined. No differences in electrical properties among deposits prepared using any of the sources are evident, however, as may be seen by comparing the data for runs SC5, SC11 (Table II, Quarterly Report No. 1) and SC17, made under otherwise similar conditions. That this result may be fortuitous is indicated by the data from the monitor Hall bars, discussed below, which show differing kinds of segregation and, therefore, possibly quite different sets of impurities.

Unfortunately, samples from SC5 and SC11 were not suitable for solar cell fabrication so that a direct comparison of solar cell

properties is not possible, and the variety of results obtained with the other samples precludes drawing of any valid conclusions.

The source of Ga has been found to influence the electrical properties, as expected, since impurities in a GaP source should be reincorporated in the epitaxial deposit. This is illustrated by the results for runs SC14 and SC15, the net carrier level of SC14-3 being the lowest evaluated while SC15-3 could not be evaluated, presumably because of nonhomogeneity of type. (Although Te doping was attempted in this run as is indicated in the table, a negligible amount, if any was transferred). Of the other two runs made with this source, SC12 and SC13 (Table II Quarterly Report No. 1) SC13 could not be evaluated either, while the higher carrier level of the SC12 deposits might be attributed to the high temperature of deposition (which might also be related to the segregation of impurities discussed below).

Measures to purify the HCl, inclusion of a U-tube trap containing HgCl_2 and $\text{Mg}(\text{ClO}_4)_2$ to remove H_2S and water (runs SC14-SC24) and immersion of the trap in a dry ice slurry (runs SC20-SC24), produced no obvious effect on the electrical properties, but in most of the runs any effect would have been masked by the deliberate Te doping. There was, however, no marked improvement in mobility to indicate a higher level of purity attained. A possible exception is the change in bump habit on undoped layers from "rounded rectangular" (Figure 1 (a)) to "square pyramidal" (Figure 1 (b)), first noticed in run SC24. Since introduction, with run SC25, of a new HCl source and a shorter, cleaner metering system, but with no further purification, carrier levels in the mid 10^{16} cm^{-3} range have been obtained (though perhaps due to other factors) and the bump habit has been "square pyramidal" as in run SC24. Whether this represents an improvement in purity is still open to question as will be discussed below. However, the new system is cleaner. A

yellow fluffy deposit which had always previously formed on the gallium source has not been obtained since introduction of the new HCl supply.

The segregation of impurities reported in Quarterly Report No. 1 has again been noticed in all runs including those heavily doped with tellurium (Table IV). As before, the net carrier level of the epitaxial layer decreases with position downstream. The persistent recurrence of an accompanying drop in mobility in the undoped series of runs indicates that the trend is real and due to an increase in a compensating p-type impurity. This is in agreement with an observed darkening of the deposit on the wall downstream which indicates an increasing impurity level. The effect could be due to silicon (known to be present in the phosphorus) which though normally a donor impurity in GaP, under the epitaxial deposition conditions could enter also as an acceptor. Thus the large decrease in mobility relative to the modest drop in carrier level could be accounted for. This large drop in mobilities did not occur in the earlier undoped runs. A possible explanation is that the new phosphorus does introduce a higher level of some impurity, perhaps silicon, having a high "segregation" coefficient. A large increase in mobility was noted in run SC5 (Table III Quarterly Report No. 1), the run made using impure phosphorus, indicating possibly an even different set of impurities.

The decreasing carrier level for the runs heavily doped with tellurium, accompanied by the small but again persistent increase in mobility shows the trend here is due to a decrease in the concentration of the n-type dopant, tellurium.

It is interesting to note that the best average mobility (indicating least compensation) has been obtained in SC30, known to be at least partially compensated with zinc.

The wide variation in net carrier levels and correlation of carrier level with growth rate noted in Quarterly Report No. 1 is probably related to this segregation effect since the relative rate of incorporation of impurities can be expected to vary with growth rates.

E. Conclusions

Although not yet fully demonstrated, it appears that growth rates in excess of $0.5 \mu/\text{min.}$ can be achieved in the open tube system while maintaining good structure. This growth rate will permit thick self-supporting layers to be grown in a reasonable time.

Smooth surfaced epitaxial layers free of major defects can be obtained by using slightly off $\langle 100 \rangle$ orientation substrate surfaces with present cleaning technique and at moderate doping levels. At the highest doping levels this may not be possible.

Doping with tellurium and zinc has been demonstrated but not fully developed.

Purity of the epitaxial GaP is less than adequate, and a number of different impurities are indicated as responsible, oxygen and silicon being chief suspects.

IV. SOLAR CELL FABRICATION

In the fabrication of solar cells attention has been directed toward three aspects (1) the improvement in junction quality, (2) the variation in zinc concentration to alter the surface concentration, and (3) the variation in junction depth.

Initial attempts to improve the junction planarity by pretreating the GaP samples with gaseous phosphorus or arsenic at 1000° C for 20 hours (with phosphorus at 10 atmospheres pressure and arsenic at 10 atmospheres pressure) prior to a zinc diffusion (see Table V - NA17, NA18a, NA18B) have not been successful. While observation of the junction front following the zinc diffusion apparently shows a more planar junction front, this is deceiving since (1) the open circuit voltage obtained is extremely low and (2) by carefully probing the layers and comparing the pretreated material before and after zinc diffusion a high resistive almost insulating layer, presumably connected with the phosphorus or arsenic used was found between the zinc diffused region and the n-type starting material. Additional diffusion of zinc for longer time to penetrate this barrier results in non-uniform junctions since in certain regions the penetration is greater than in others. Solar cell characteristics showed no improvement.

Better junction fronts and also higher open circuit voltages have resulted from improvement in the technique for making the epitaxial GaP and a resultant improvement in the structure of the GaP. The junctions now appear to be more uniform with little or no evidence of spikes.

Efforts are being made to optimize the surface concentration by varying the amount of zinc placed in the diffusion tube. Thus far, the results, as deduced from Hall and resistivity measurements of the surface concentration, are not clear. The results presently available are tabulated in Table VI for two representative lots of material. It is acknowledged that the amount of zinc used in these experiments may still be too high and for this reason additional experiments using, perhaps, gallium-zinc

alloys should be performed in order to reduce the zinc concentration further.

It is noted in Table VI that reducing the amount of zinc added to the diffusion tube below 0.5 mg appears to have had no effect on the resultant surface concentration. Further, the observed junction depths do not show any consistency as the zinc concentration was reduced.

The diffusion cycle, which for normal testing of material consists of a short zinc diffusion with the resultant formation of a shallow p-n junction, was varied as shown in Table VII to see whether the diffusion followed the analytical predictions of G. L. Pearson¹ and to test the effect of deeper junctions on solar cell characteristics (these will be described later).

Reasonable agreement was found for the diffusion coefficient of zinc as deduced from these experiments and what would be predicted from Pearson's analysis.

Of general concern, however, was the fact that the diffusion depth as found from etching and delineation techniques described in the first quarterly report^{*}, for certain samples having higher initial carrier concentrations, was deeper than for those of lower initial carrier concentration. Both types of samples were run with the same amount of zinc, same temperature and time. At this time these findings are not understood but it may be related to the fact that most of the starting materials are compensated to some degree.

It has been observed that starting material which was initially p-type gives rise to a p-n junction when zinc is diffused (shallow) into it. This was particularly true of samples SC13-4 and SC21-3.

* See Page 10, Quarterly Report No. 1

V. SOLAR CELL EVALUATION

The room temperature solar cell characteristics of open circuit voltage and short circuit current density are given in Table VIII for the samples fabricated during this period, together with the cell area evaluated and the spectral response peaks in microns. The fabrication techniques and apparatus have been described in the first quarterly report.

Highest open circuit voltage observed has been 1.18 volts. This has been observed on several samples and a good number of others have open circuit voltages of 1.0 volt or higher. In all these cases the short circuit current density is about 0.1 ma/cm^2 or less. The samples are further characterized by having a spectral response approximating the direct and indirect band to band transitions². On the other hand, highest short circuit current densities found have been for sample NA21-SC21-3 with a room temperature value of 5 ma/cm^2 . A mesa of sample NA16 SC13-6 gave a value of 2 ma/cm^2 . The open circuit voltage of NA21-SC21-3 was 0.74 volts. Of further striking interest is the fact that the major response appears to be at the longer wavelengths.

In order to further verify that the results obtained on NA21 SC21-3 was associated with GaP, a response curve was taken of the starting material SC21-3, using a gold dot on the surface and an alloyed Au-Sn Kovar back contact, and it showed definite spectral response features characteristic of GaP³, i. e., response peaks at $\sim 0.46 \mu$ and 0.56μ . Hence the shift in response on fabrication as deduced from these results appears to be related to the diffusion process and/or heat treatment.

These longer wavelength responses are really broad bands rather than sharp peaks. In the interest of simplicity we shall refer to the longer wavelength response as a $.7 \mu$ band. The shift in response and the respective short circuit current densities observed will be covered in more detail later. The highest conversion efficiency has been attained with NA21-SC21-3 where a value of 2.5% has been observed. The current density at maximum

power was 4.5 ma/cm^2 and the corresponding voltage was 0.56 volts. Samples tested have had cell areas of about $.2 \text{ cm}^2$ as seen in Table VIII.

For those samples having the main response peaks at 0.45 to 0.53μ , the highest short circuit current density obtained has been about 0.2 ma/cm^2 . This is in sharp contrast with the above results.

A. Bump Density

Efforts have been made to determine whether imperfections of the type shown in Figure 2b and hereafter identified as bumps can in some manner be correlated with the measured electrical characteristics. Since all material presently made has these imperfections on the surface, a count has been taken of them and recorded in terms of the number of bumps per cell area. The last column in Table VIII contains the bump density for some of the fabricated solar cells. No obvious correlation exists between the bump density and the open circuit voltages.

B. Spectral Response Measurements

As already shown in Table VIII the spectral response in the range of $0.45 - 0.55 \mu$ predominates for those samples with relatively low short circuit current densities. The higher short circuit density samples appear to have their main response at wavelengths $> 0.58 \mu$ and centered roughly around 0.7μ . In Table IX we have given the magnitudes of the spectral response peaks using a Reeder thermocouple as a reference standard. (The magnitude of the peaks are given in terms of $\mu \text{ a} / \mu \text{ v}$ where the $\mu \text{ v}$ represents the voltage output of the thermocouple which can be related to a thermocouple energy using the standard - $.46 \mu \text{ w} / \mu \text{ v}$). The solar cells in this table have all been made by the same standard diffusion cycle as noted in Table V. Of interest is the fact that those samples which have been doped with tellurium show very strong response at 0.45 (and 0.50μ) with a decided absence of response at wavelengths $> 0.55 \mu$. On the other hand several samples show a decidedly greater response at about 0.7μ (band) with smaller or no response at the shorter wavelengths. We will further

examine these observations in the discussion.

C. Photo Response of Top Metal Contact to GaP Solar Cell

To attempt to explain the deviation between observed open circuit voltages (~ 1.2 volts) and the theoretical (~ 1.5 volts) the effect of the photo voltage generated by the top metal contact (silver) of the GaP solar cells was investigated. Successive masking of the contact and the surface of the solar cell with black wax has led to no change in open circuit voltages within the error of the experiment as can be seen from Table X. It has been concluded that the effect of the metal contact to the GaP does not affect the open circuit voltage obtained and hence cannot explain the low open circuit voltages obtained from the fabricated GaP solar cell.

D. Effect of GaP-GaAs Interface

To further examine the possibility that the GaP-GaAs interface might be influencing solar characteristics another experiment was carried out. This consisted of taking a zinc diffused unit, NA25-SC24-5, and etching out a portion of the GaAs to provide a window directly to the back of the GaP layer. The GaAs was masked with black wax except for the portion to be etched away. The etch used consisted of 1 HF: 3 HNO₃: 2 H₂O. This etch only negligibly attacks GaP.

A sketch of the etched sample is shown in Figure 4. Contact 2 is the original back contact of Au-Sn-Ni, contact 3 is made by using a mica mask of diameter smaller than the "window" and evaporating Au-Sn-Ni. This sample is heated to 400° C following the evaporation as is normally carried out for the back contact. The top contact (1) employs evaporated silver.

The short circuit current and open circuit voltages were measured under various conditions: (1) with a microscope light and the window in the up position, (2) under normal solar cell testing conditions in our standard test apparatus with the front face of the GaP (with silver contact) facing the light source and the window in the back.

We compared the Ag-Au-Sn-Ni (GaAs) contact with the Ag-Au-Sn-Ni (GaP) contact. The former contact includes the GaP-GaAs interface, the latter does not. Both the measurements of open circuit voltages and short circuit current produced identical values for these contacts under condition 2 and they were the same under condition 1. This experiment further corroborates our earlier experiments described in the first quarterly report wherein we concluded that in our present material the GaP-GaAs interface does not play a significant role in determining the characteristics of the GaP solar cell.

E. Solar Cell Characteristics as function of Temperature

The short circuit current density and open circuit voltages of a number of fabricated GaP solar cells shown in Tables V and VIII have been measured as a function of increasing temperature. Solar measurements have been made using a tungsten light source with the samples placed in a furnace. The results are tabulated in Table VII where the room temperature values are displayed as well as the temperature where the short circuit current density appears to reach its highest value. At this same temperature the open circuit voltage is also given. Typical curves of the short circuit current density and open circuit voltage as a function of temperature are shown in Figures 5, 6 and 7.

It has been observed that the open circuit voltage decreases fairly rapidly with increasing temperature. The rate of decrease is typified by two types of change; those that appear to show a decrease in voltage to half the initial value at a temperature of 150-175° C and those which decrease to half their starting value at a temperature of about 250° C. The short circuit current density on the other hand generally increases with temperature. Thus far, high J_{sc} at elevated temperatures has been observed for samples NA16 SC13-6 (3.7 ma/cm² at 300° C), NA20 SC13-4 (0.97 ma/cm² at 300° C) and for sample NA21 SC21-3, which has shown little change in J_{sc} (4.5 ma/cm²) with temperature to ~ 200° C. In the case of sample NA16 SC13-6 a rise

of 2 orders of magnitude occurred on going from room temperature to 300° C. On the other hand the open circuit voltage drops to only .020 volts from a starting value of .58 volts at room temperature.

The slopes associated with the short circuit current density from the relationship $J_{sc} \sim e^{-\Delta v/kT}$ are of interest for there appear to be five slopes which characterize the measured samples:

$$\Delta v = 0 \text{ ev}$$

$$\Delta v = 0.04 \text{ ev}$$

$$\Delta v = 0.08 \text{ ev}$$

$$\Delta v = 0.3 \text{ ev}$$

$$\Delta v = 0.5 \text{ ev}$$

Sample NA 21 SC21-3, which has a J_{sc} of about 5 ma/cm² and a very strong spectral response at $\sim 0.7 \mu$ wavelength at room temperature exhibits zero slope to $\sim 200^\circ \text{C}$. The slopes 0.04 and 0.08 ev are found for those samples which are characterized at room temperature by spectral response in the region of about 0.45 - 0.55 μ . Slopes 0.3 and 0.5 ev are noted for those samples which have some small response at wavelengths $> .55 \mu$ ($\sim .7 \mu$) at room temperature. While it is believed that these slopes should be correlated with an impurity level, this point has not yet been established.

F. Diffusion Length Measurements

Using the method of Logan and Chynoweth⁴, room temperature measurements of diffusion length have been made on mesas of some of the solar cells to determine whether the low short circuit currents observed can be correlated with the measured diffusion lengths. A plot of $\frac{1}{C/A}$ (capacity/area)⁻¹ vs. J_p (photo current density of the cell with reverse bias) from which a value of L_D , the minority carrier diffusion length, can be deduced is shown in Fig. 8 for sample NA16 SC13-6. Some values obtained by this method are shown in Table XII. Because of competing mechanisms the results may be regarded as upper limits.

Diffusion lengths measured have ranged from about 450 \AA to about 5000 \AA . Using a carrier diffusion constant of $2.5 \text{ cm}^2/\text{sec}$. the values of the diffusion length correspond to values of minority carrier lifetime varying from 10^{-12} to 10^{-10} sec. It is also likely that the lifetime of electrons in the heavily doped p layer (zinc diffused) may even be several orders of magnitude below these measured values. In fact, some of the samples such as the mesa of NA 16 SC13-6 which has a spectral response in the 0.7μ region and has a room temperature short circuit current density of 2 ma/cm^2 has a very short diffusion length of $\sim 150 \text{ \AA}$. (This is one of the samples where the sensitivity of the measurements was good). This last example is also the basis for regarding some of the diffusion length measurements with caution and also suggesting that competing processes or mechanisms can be occurring in the solar cell which may lead to erroneous interpretation of the diffusion length measurements.

Several questions are raised by the values of diffusion length given in Table XII. If a diffusion length of the order of 150 \AA is taken as an estimate of minority carrier diffusion length, then it can account for the low short circuit current densities obtained with samples which have primary spectral response in the wavelength range of $0.45 - 0.55 \mu$. However, it is difficult to understand why those samples which respond to the 0.7μ region should have considerably higher short circuit currents (regardless of carrier generation mechanism) especially if the diffusion length could be a limiting mechanism. In order to more clearly view this question it is perhaps well to examine the nature of the p-n junction through current-voltage characteristics and capacity-voltage measurements.

G I-V Characteristics

The I-V characteristics of these solar cells as can be seen from

Table XII shows that $n > 2$ in the I-V relationship

$$I = I_0 \exp \left(\frac{eV}{nkT} - 1 \right). \quad (1)$$

The I-V relationship with $n > 2$ suggests the presence of recombination centers⁵ as has already been noted in the previous report. In Fig. 9 is shown an I-V trace at room temperature for sample NA24 SC13-6 where there is evidence of a negative resistance region in the forward characteristic of the trace.

H. Capacity-Voltage Measurements

Capacity-voltage measurements taken on mesas of the fabricated solar cells generally support the idea that the p-n junctions are graded and appear to follow a $1/C^3$ law as seen in Table XII. Figure 10 shows a plot of the capacity vs voltage for sample NA 21SC19-5. It appears to follow the $1/C^3$ law. It has been possible to fit, generally, the capacity-voltage data to the following types of equations:

$$V_a + V_i = - \frac{qa}{12 \epsilon} \left(\frac{\epsilon}{C/A} \right)^3 \quad (2)$$

$$V_a + V_i = - \frac{qa}{12 \epsilon} \left(\frac{\epsilon}{C/A} - W_I \right)^3 \quad (2a)$$

$$V_a + V_i = - \frac{qa}{12 \epsilon} \left(\frac{\epsilon}{C/A} - W_I \right)^2 \left(\frac{\epsilon}{C/A} + \frac{W_I}{2} \right) \quad (2b)$$

where V_a is the applied reverse voltage, V_i is the built in voltage of GaP, a constant and characteristic of the material. For n-type GaP we have taken $V_i = 2$ volts in order to fit the data. (This agrees with the results of White and Logan⁶ and Logan and Chynoweth⁴. In the equations q is the electronic charge, ϵ the dielectric constant, C the capacity of the junction, A the cross sectional area of the junction and a is a concentration gradient in the graded junction. W_I is introduced into the equations to fit our experimental results and it signifies that the space charge layer of the junction is extremely wide and infers that the space charge layer is intrinsic so that we may in these samples talk about a p-I-n cell. In Table XII reference is made to calculations

from the data using eqs. 2-2b. One notes that some of the samples with higher short circuit current densities have smaller "I" layers and also the diffusion length is greater than the "I" layer. This is especially true for mesa sample NA 16 SC13-6.

The "I" layer or W_I as calculated for the samples in Table XII is seen to vary from 150 Å to about 10 μ . The gradient, a , is observed to generally decrease with increasing width of I layer.

The mesas which have been used in these measurements generally have areas in the range of 10^{-3} cm^2 .

It remains to attempt to correlate the short circuit current density, open circuit voltage, spectral response, diffusion length, capacity-voltage measurements into a single picture.

J. Effect of Junction Depth on Solar Cell Characteristics

In Table XIII is given the results of an investigation on the effect of deeper junctions on the solar cell characteristics. Diffusions with samples SC13-6 to SC21-3 were carried out with both shallow ($\sim 0.5 \mu$) and deeper penetrations (3-5 μ). The results show agreement with what one expects from general solar cell theory. The open circuit voltage is independent of the junction depth while the short circuit current density decreases using the deeper junction. The results of this investigation would support the use of a shallow junction as opposed to a deep junction.

VI. DISCUSSION

The experimental results obtained thus far on epitaxial GaP solar cells suggest that the cells presently made fall into two categories:

- (a). those with high open circuit voltage and low short circuit currents
- (b). those with high short circuit currents and low open circuit voltages.

The highest conversion efficiency has been obtained from the latter category. The optimum features of each type have not yet been successfully combined nor has theoretical expectations for J_{sc} and V_{oc} been achieved. It may be of interest to discuss these in more detail.

A. Open Circuit Voltage

The highest open circuit voltage obtained at room temperature is 1.2 volts. This begins to approach the theoretical value of 1.5 volts. Attempts to associate the difference with the effects of the top metal-p layer semiconductor contact or the GaP-GaAs substrate interface have been negative. The clearest association appears to relate the difference to the nature of the junction formed, and this includes not only the physical junction, i. e., whether the junction front is physically flat and planar but refers also to the electrical nature of the junction, i. e., whether the junction is graded with a relatively wide space charge layer and the nature of the impurities in this layer. This point has also been raised by LaMorte⁷ for GaAs solar cells.

Our present information does not provide us with a detailed enough description of the space charge region to speculate on the types and nature of the centers present there.

B. Short Circuit Current Density

The spectral responses at about 0.45μ and about 0.53μ

correspond to the two conduction band minima in GaP^2 at about 2.7 eV and 2.3 eV. From Table IX, the response at the higher energy corresponding to the direct gap is larger than the response at the indirect, lower energy conduction minimum for those cells exhibiting no response at still longer wavelengths. The low values of short circuit current arising from these band edge responses appear to be primarily associated with short minority carrier lifetimes and diffusion lengths. This statement draws support from the diffusion length measurements listed in Table XII and discussed earlier. If one assumes a diffusion coefficient of about $2.5 \text{ cm}^2/\text{sec}$ for holes or electrons, then τ , the lifetime may be of the order of 10^{-12} sec. This is not unexpected in a wide band gap material where a variety of impurity levels both shallow and deep are possible with varying combinations of trapping and recombination processes likely.

Many of the cells show a pronounced response in the region of 0.7 microns and in these cells, little or no response is exhibited at the band edge. In fact, the highest spectral response observed so far has been in this longer wavelength region. Since the energy corresponding to a wavelength of 0.7μ (1.8 e.v.) is less than the band gap, photoresponse with light of this energy must involve a two-step excitation, with two optical steps or one optical and one thermal step. The interband level involved may be the deep donor level (0.4 e.v.) attributed to oxygen by Gershenzon and Mikulyak⁸. The greater photocurrent generated in these cells by the 0.7μ light may arise from carrier trapping effects resulting from the nature of the impurity centers, the Fermi level and the details of the excitation process. Preliminary attempts have been made to construct models which might explain these effects.

VII. FUTURE STUDIES

The efforts to grow thick layers of GaP will be continued by using higher flow rates, higher temperature gradients and reducing or eliminating the deposition on the wall by revising the temperature gradient between the substrate and the adjacent wall.

Efforts to eliminate structural defects by improving the cleaning procedure and optimizing run conditions (within limits to obtain a rate of $0.5 \mu/\text{min}$) will be continued. A light oxidation of the surface might remove organic contaminants and subsequently be removed in the phosphorus vapor pretreatment process.

The principal run conditions to be optimized are purity of the reaction gases and phosphorus pressure control.

The purity of the gallium phosphide must be improved. An attempt will be made to identify the principal active impurities by spectroscopic analysis. A source of pure phosphorus must be obtained and the HCl should be purified. The behavior of suspect impurities such as oxygen and silicon should be established.

The effect on purity as reflected in solar cell properties of such run conditions as phosphorus pressure and H_2 flow rates will be investigated more systematically.

Techniques for doping with tellurium, selenium, and zinc to control net carrier level will be perfected. Doping with the Group IV elements, Si, Ge and Sn, will be investigated.

The contributions of the band edge to the current is extremely small and the reasons not clear. It is of value to investigate the absorption in the p layer, surface recombination effects and the effects of the surface concentration on the short circuit current density.

The reason for the large current response from the 0.7μ wavelength is not clear. It is planned to look into the mechanism. It is important to determine why lifetime does not inhibit this response. It is

also of importance to determine where the level is coming from, what impurities may be involved.

Hall measurements on the epitaxial GaP samples will be carried out in an attempt to determine some of the shallow level impurities present in the epitaxial GaP material and a closer correlation of the solar cell properties and the material deposition parameters will be attempted.

It is planned to study the space charge region in more detail and see whether this can be related to (a) the large response of the 0.7μ wavelength and (b) the poor response of the absorption edges.

It would be of interest to examine some of the non-radiative and radiative processes in the epitaxial GaP.

VIII. REFERENCES

1. G. L. Pearson, private communication.
2. W. Spitzer, M. Gershenzon, C. J. Frosch and D. F. Gibbs, J. Phys. and Chem. Solids, 11 , 339 (1959).
3. H. C. Grimmeiss, A. Rabenau and H. Koelmans, J. A. P. , 32 , 2123 (1961).
4. R. A. Logan and A. G. Chynoweth, J. A. P. , 33 , 1649 (1962).
5. Sah, Noyce, Shockley, Proc. IRE, 45 , 1228 (1958).
6. H. G. White and R. A. Logan, J. A. P. , 34 , 1990 (1963).
7. M. F. LaMorte, Advanced Energy Conversion, 3 , 551 (1963).
8. M. Gershenzon and R. M. Mikulyak, J. A. P. , 32 , 1338 (1961).

APPENDIX A

Estimates have been made of the amount of solar energy greater than 2.2 e.v. which is absorbed in GaP as a function of the thickness of GaP. In these calculations the absorption coefficient was approximated from the measurements of Spitzer, et al ² and assumed to vary as the square of the photon energy, i.e., $\alpha(E) = A(E - E_0)^2$. Here $\alpha(E)$ is the absorption coefficient at a particular photon energy, A is a constant to be fitted ($A = 6.25 \times 10^3 \text{ cm}^{-1}/\text{ev}$), $E_0 = 2.2 \text{ e.v.}$ The number of photons available as a function of energy ($> 2.2 \text{ e.v.}$) was approximated from the available data on the solar spectrum in the energy range of interest for GaP ($> 2.2 \text{ e.v.}$) by a parabola having the following form:

$$n(E) = n_0 - \gamma(E - E_1)^2$$

where $n(E)$ are the number of available photons as a function of energy, n_0 , γ , E , are constants. The equation with the appropriate constants was found to be

$$n(E) = 3.5 \times 10^{17} - 2.43 \times 10^{16}(E-1)^2$$

The results of the calculations are plotted in Figure 11.

These approximate calculations indicate that for a GaP thickness of 15 microns about 80% of the energy > 2.2 should be absorbed.

APPENDIX BEquipment

A new grating blazed for 0.5 microns has been installed in the Bausch and Lomb monochromator this period and suitable calibrations carried out.

A leakage tester with input impedance of 10^{11} ohms has been built to check reverse characteristics.

Equipment to measure solar cell characteristics as a function of temperature has been built and put to use.

TABLE I
Epitaxial Deposition of GaAs

Run and Sample No.	Source	Source Temp (°C)	Substrate		Flow Rates (cc/min)			Time (min.)	Thickness μ	Growth Rate	
			Position (in.)	Temp (°C)	HCl	H ₂	P ₄			(μ /min)	μ /cc HCl
SC21	Ga, Te + P	890	14	815	0.92	15	2.0	243	10*	.04	.04
SC25	Ga + P	890	14	815	1.1 (1.47)	150	< 0.3	720	40	.06	.05
SC26	Ga + P	975	14-1/2	820	1.5 (1.46)	150	< 0.3	661	45	.07	.05
SC17	Ga + P	890	14-1/2	810	1.2	150	1.1	240	25	.10	.09
SC27	Ga + P	890	14 **	815	0.85(1.14)	170	1.3	240	25	.10	.12
SC18	Ga + P + Te	890	{ 14-1/4 15-1/4 }	{ 814 805 }	1.0	150	1.2	240	{ 26 20 }	{ .11 .08 }	{ .11 .08 }
SC28	Ga + P	890	14 **	815	0.93(1.16)	170	1.2	280	35	.12	.13
SC14	GaP + P	890	14	815	0.85	150	2.7	240	30	.12	.15
SC19	Ga + P + Te	890	{ 14-1/2 15-1/2 }	{ 810 803 }	0.88	150	2.1	243	{ 34 25 }	{ .14 .10 }	{ .16 .12 }
SC20	Ga, Te + P	890	14	815	1.1	300	1.4	281	43	.15	.14
SC23	Ga, Te + P	890	14	815	1.4	500	1.7	133	21	.16	.11
SC15	GaP + P + Te	890	14-1/4	812	0.88	150	2.3	244	40	.16	.19

TABLE I (Continued)
Epitaxial Deposition of GaAs

Run and Sample No.	Source	Source Temp (°C)	Substrate		Flow Rates (cc/min)			Time (min.)	Thickness μ	Growth Rate	
			Position (in.)	Temp (°C)	HCl	H ₂	P ₄			(μ /min)	μ /cc HCl
SC29	Ga + P + Zn	975	15-1/2	795	0.94(1.14)	150	1.2	270	55	.20	.22
SC16	GaP + P + Te	890	14-3/4	807	1.1	150	1.4	240	50	.21	.19
SC24	Ga + P	890	{ 14 15 }	{ 815 805 }	2.4	500	1.1	245	{ 70 57 }	.29 .23	.12 .10
SC22	Ga, Te + P	890	14	815	1.5	500	3.5	50	15	.30	.20
SC30	Ga, Zn + P	975	15	810	{ 0.9 2.1 (2.35) }	170	1.1 1.1	{ 10 248 }	95	.38	.18

* Very ragged interface

** Wafer supported vertically with both sides exposed

TABLE II
Properties of Undoped GaP Epitaxial Layers (n-type)

<u>Sample No.</u>	<u>Source</u>	<u>Thickness, μ (Approx.)</u>	<u>ρ</u>	<u>μ</u>	<u>n</u>
SC14-2	GaP + P	30	110	63	9.7×10^{14}
SC15-3	GaP + P + Te (?)	40	non ohmic contacts		
SC17-3	Ga + P	25	1.2	68	1.4×10^{17}
SC24-3	Ga + P	70	.10	88	7.3×10^{17}
SC24-5	"	57	.14	89	5.1×10^{17}
SC25-3	"	40	13.4	68	2.5×10^{16}
SC26-3	"	45	2.4	74	3.6×10^{16}
SC27-3	"	25	2.7	74	4.8×10^{16}
SC28-3	"	35	3.2	88	2.7×10^{16}

TABLE III
Tellurium and Zinc Doped GaP Epitaxial Layers

<u>Sample No.</u>	<u>Source</u>	<u>Thickness, μ (Approx.)</u>	<u>ρ</u>	<u>μ</u>	<u>n</u>
SC16-3	GaP + P + $3.0 \times 10^{19} \text{ cm}^{-3} \text{ Te}$	50	.017	32	1.9×10^{19}
SC18-3	Ga + P	26	.29	55	5.3×10^{17}
-5	+ $1 \times 10^{18} \text{ cm}^{-3} \text{ Te}$	20	.66	53	2.0×10^{17}
SC19-3	Ga + P	34	.23	46	6.2×10^{17}
	+ $1.3 \times 10^{19} \text{ cm}^{-3}$	25	.59	38	3.8×10^{17}
SC20-3	Ga, Te reused + P	43	.052	79	1.5×10^{18}
SC21-3	"	10*	non ohmic contacts		
SC22-3	"	15	.046	45	3.2×10^{18}
SC23-3	"	21	.043	47	3.1×10^{18}
SC29-3	Ga + P + Zn (350°)	55	.037	(25)	$(6 \times 10^{18}) \text{ (p)}$
SC30-3	Ga, Zn reused + P	95	2.4	96	$3.2 \times 10^{16} \text{ (n)}$

* very ragged interface, non-standard growth conditions

TABLE IV
Segregation of Impurities with Substrate Position

Run No.	Hall Bar	Carrier Density			Mobility		
		1st	2nd	3rd	1st	2nd	3rd
SC29	(Zn doped)	(n)?	6.6×10^{18} (p)		-	26	
SC14		1.1×10^{15}	8.6×10^{14}		89	47	
SC26		3.6×10^{16}	-		74	-	
SC28		3.7×10^{16}	1.6×10^{16}		95	82	
SC25		4.2×10^{16}	7.7×10^{15}		103	32	
SC30	(Zn doped?)	4.3×10^{16} (n)	2.1×10^{16} (n)		103	90	
SC27		6.4×10^{16}	3.2×10^{16}		105	44	
SC17		2.5×10^{17}	4.7×10^{16}		72	63	
SC19	(Te doped)	7.0×10^{17}	5.4×10^{17}	2.1×10^{17}	52	40	35
SC18	(Te doped)	8.0×10^{17}	2.5×10^{17}	1.5×10^{17}	51	59	47
SC24		9.1×10^{17}	5.6×10^{17}	4.6×10^{17}	93	83	94
SC20	(Te doped)	1.7×10^{18}	1.4×10^{18}		78	80	
SC23	(Te doped)	3.3×10^{18}	3.0×10^{18}		46	49	
SC22	(Te doped)	3.9×10^{18}	2.5×10^{18}		44	46	
SC16	(Te doped)	2.9×10^{19}	9.0×10^{18}		29	36	

TABLE V
Solar Cell Fabrication
Diffusion Data

Diff. Run No.	Slice No.	Diffusant Source and Amt.	Diff. Temp (°C)	Diff. Time (Min.)	P Surface Conc/cm ³	μ of P Layer cm ² /volt sec.	Junction Depth μ
NA-14	bulk, poly	5.8 mg Zn, 1.8 mg P	800	3	-	-	-
NA-15	bulk, poly (old)	1.1 mg Zn	800	3	-	-	-
	bulk, poly	1.1 mg Zn	800	3	1.9x10 ¹⁹	30	-
	(Lot 170)						
NA-16	SC 6/11-3	5.8 mg Zn, 1.8 mg P	800	3	1 x 10 ¹⁹	-	0.5
	SC14-2	"	800	3	4.2x10 ¹⁸	36	1.5
	SC13-6	"	800	3	1 x 10 ¹⁹	-	≤ 0.5
NA-17	SC6/11-3	*5.8 mg Zn, 1.8 mg P	800	3	high ρ	-	< 0.5
NA-18a	SC6/11-3	** 1 mg Zn ₃ As ₂ in .3 ml volume tube	900	4	high ρ	-	1.5
NA-18b	SC6/11-3	*** 5.8 mg Zn	800	30	1.4-3 x 10 ¹⁹	-	7-15
NA-20	SC13-4	5.8 mg Zn, 1.8 mg P	800	3	1.5x10 ¹⁹	58	0.5
NA-20	SC15-3	"	800	3	1.5x10 ¹⁹	81	≤ 0.5
NA-20	SC16-3	"	800	3	-	-	< 0.5
NA-20	SC17-3	"	800	3	9.9x10 ¹⁸	37	< 0.5
NA-21	SC18-3	"	800	3	6.4x10 ¹⁸	28	< 0.4
NA-21	SC18-5	"	800	3	4.9x10 ¹⁸	63	< 0.4
NA-21	SC19-3	"	800	3	8.5x10 ¹⁸	31	< 0.4
NA-21	SC19-5	"	800	3	7.5x10 ¹⁸	37	< 0.4
NA-21	SC20-3	"	800	3	7 x 10 ¹⁸	22	0.4
NA-21	SC21-3	"	800	3	1.3x10 ¹⁹	66	< 0.4
NA-22	SC13-6	"	800	10	1.2x10 ¹⁹	35	3
NA-22	SC13-4	"	800	10	1.2x10 ¹⁹	30	3
NA-22	SC19-5	"	800	10	7 x 10 ¹⁸	27	5
NA-22	SC17-3	"	800	10	8.8x10 ¹⁸	24	5
NA-22	SC21-3	"	800	10	1.1x10 ¹⁹	31	4
NA-23	SC13-6	.5 mg Zn, 1.8 mg P	800	3	5 x 10 ¹⁸	78	< 1

TABLE V (Continued)
Solar Cell Fabrication
Diffusion Data

Diff. Run No.	Slice No.	Diffusant Source and Amt	Diff. Temp (°C)	Diff Time (Min.)	P Surface Conc/cm ³	μ of P Layer cm ² /volt sec.	Junction Depth μ
NA-23	SC19-3	.5 mg Zn, 1.8 mg P	800	3	2.3×10^{18}	21	2
NA-23	Ct VIII (closed tube)	"	800	3	-	-	1
NA-24	SC13-6	.1 mg Zn, 1.8 mg P	800	3	6×10^{18}	89	< 0.5
NA-24	SC19-3	"	800	3	3×10^{18}	-	0.7
NA-25	SC22-3	5.8 mg Zn, 1.8 mg P	800	3	6.1×10^{18}	37	0.7
NA-25	SC23-3	"	800	3	7×10^{18}	29	0.7
NA-25	SC24-3	"	800	3	5.6×10^{18}	30	0.7
NA-25	SC24-5	"	800	3	6.3×10^{18}	30	0.7
NA-25	SC25-3	"	800	3	4.0×10^{18}	30	1.5
NA-25	SC26-3	"	800	3	3.4×10^{18}	42	1.5

* Pretreated with arsenic vapor at 10 atmospheres at 1000° C for 20 hours

** Pretreated with phosphorus vapor at 10 atmospheres at 1000° C for 20 hours

*** Previous sample diffused additionally

TABLE VI
Variation in Surface Concentration with Zinc Concentration

Run No.	Sample No.	Carrier Conc., N	Diffusant* Source and Amt.	P Surface Conc	Mobility of P Layer	Junction Depth (μ)
NA-16	SC13-6	1×10^{17}	5.8 mg Zn 1.8 mg P	1×10^{19}	-	< 0.4
NA-23	SC13-6	1×10^{17}	.5 mg Zn 1.8 mg P	5×10^{18}	78	< 1
NA-24	SC13-6	1×10^{17}	.1 mg Zn 1.8 mg P	6×10^{18}	78	< 0.5
NA-21	SC19-3	6.2×10^{17}	5.8 mg Zn 1.8 mg P	8.5×10^{18}	31	< 0.4
NA-23	SC19-3	6.2×10^{17}	.5 mg Zn 1.8 mg P	2.3×10^{18}	21	2
NA-24	SC19-3	6.2×10^{17}	.1 mg Zn 1.8 mg P	3×10^{18}	-	0.7

* All diffusions were carried out at 800° C for 3 minutes.

TABLE VII
Variation in Diffusion Depth

Run No.	Slice No.	Diffusant Source and Amt.	Diff. Temp °C	Diff. Time Min.	P-Surface Conc / Cm^3	Junction Depth μ
NA-16	SC13-6	5.8 mg Zn, 1.8 mg P	800	3	1×10^{19}	< 0.5
NA-20	SC13-4	"	800	3	1.5×10^{19}	0.5
NA-21	SC19-5	"	800	3	7.5×10^{18}	< 0.4
NA-20	SC17-3	"	800	3	9.9×10^{18}	< 0.5
NA-21	SC21-3	"	800	3	1.3×10^{19}	< 0.4
NA-22	SC13-6	"	800	10	1.2×10^{19}	3
NA-22	SC13-4	"	800	10	1.2×10^{19}	3
NA-22	SC19-5	"	800	10	7×10^{18}	5
NA-22	SC17-3	"	800	10	8.8×10^{18}	5
NA-22	SC21-3	"	800	10	1.1×10^{19}	4

TABLE VIII
Solar Cell Evaluation Data at Room Temperature

Diff. Run No.	Slice No.	V _{oc} Volts	J _{sc} ma/cm ²	Spectral Response Peaks Microns			Cell Area cm ²	"Bump" density bumps/cm ²
				λ_1	λ_2	λ_3		
NA14	poly	.005	.12	.47	.56	-	-	-
NA15	poly	.001	.04	-	-	-	.10	-
NA15	poly	.160	.1	-	-	-	.08	-
NA16	SC6/11-3	.005	.18	-	-	-	-	-
NA16	SC14-2	1.0	.495	-	-	-	.22	-
NA16	SC13-6	.58	.01	.46	.527	.587	.06	-
						.70		
NA17	m *	.54	2.0	.58	.7(broad)	-	.0026	-
NA18a	SC6/11-3	.008	.01	-	-	-	-	-
NA18b	SC6/11-3	.0013	.01	-	-	-	-	-
NA20	SC6/11-3	.006	.013	-	-	-	-	-
NA20	SC13-4	.725	.12	.46	.54	.73	.26	-
NA20	m*	.10	1	.55	.7(broad)	-	.0035	-
NA20	SC15-3	.745	.007	.53	-	-	.27	-
NA20	SC16-3	.008	.02	-	-	-	.12	-
NA20	SC17-3	.60	.20	.53	.73(broad)	-	.19	-
NA21	SC18-3	1.18	.06	.45	.50	-	.12	11
NA21	SC18-5	1.08	.08	.45	-	-	.19	25
NA21	SC19-3	1.00	.14	.45	.50	-	.16	215
	{	.980	.16	.45	.50	-	.25	139
NA21	SC19-5	.96	.09	.45	-	-	.08	372
NA21	SC20-3	.96	.12	.45	.50	-	.13	138
NA21	SC21-3	.92	.06	.45	-	-	.25	19
NA21	SC13-6	.98	.06	.45	-	-	.18	7
NA22		.74	5.0	.77(broad)	-	-	.20	-
NA22		.65	.005	.53	.60	-	.15	-

TABLE VIII (Continued)
Solar Cell Evaluation Data at Room Temperature

Diff. Run No.	Slice No.	V _{oc} Volts	J _{sc} ma/cm ²	Spectral Response Peaks Microns			Cell Area cm ²	"Bump" density bumps/cm ²
				λ_1	λ_2	λ_3		
NA22	SC13-4	.74	.006	.46	.53	-	.15	-
NA22	SC19-5	.92	.06	.48	-	-	.15	-
NA22	SC17-3	.96	.04	.46	-	-	.19	-
NA22	SC21-3	.62	1.14	.75(broad)	-	-	.14	-
NA23	SC13-6	.72	.016	.53	.58	.7(broad)	.06	-
NA23	SC19-3	.86	.14	.45	-	-	.27	-
NA23	CTVIII	.65	.01	.46	-	-	.02	-
NA24	SC13-6	.56	.03	.53	.60	.7(broad)	.13	-
NA24	SC19-3	.25	.14	.445	.50	-	.11	-
NA25	SC22-3	{ .90 .56	.06 .04	.45 -	-	-	.36 .19	42 63
NA25	SC23-3	1.1	.06	.45	-	-	.11	109
NA25	SC24-3	{ 1.1 1.0	.06 .04	.45 -	-	-	.18 .21	39 67
NA25	SC24-5	{ 1.1 1.0	.07 .06	.45 -	-	-	.39 .06	75 69
NA25	SC25-3	{ .92 .80	.19 .15	.45 -	.50 -	-	.24 .19	121 105
NA25	SC26-3	{ .90 .92	.13 .07	.46 -	.53 -	-	.39 .21	112 157

m* - Mesa Diode

TABLE IX
Spectral Response of Solar Cells Normalized Relative to Thermocouple

Diff. Run No.	Slice No	P-Surface Conc/cm ³	Initial Base Conc(N) No/cm ³	Spectral Response Peaks Microns and Relative Intensities			
				(in ma/ μ v)			
				$\lambda_1, (\mu)$	$I_1, (\mu a/\mu v)$	$\lambda_2 (\mu)$	$I_2, (\mu a/\mu v)$
NA16	SC13-6	1 x 10 ¹⁹	1 x 10 ¹⁷	.46	.014	.53	.039
	Mesa SC13-6			-	-	-	-
NA16	SC14-2	4.2 x 10 ¹⁸	1 x 10 ¹⁵	.46	.072	.495	.5
NA20	SC13-4	1.5 x 10 ¹⁹	3.7 x 10 ¹⁶	.46	.047	.54	.176
	(P-type)						
NA20	SC15-3	1.5 x 10 ¹⁹	graded	-	-	.53	.154
NA20	SC17-3	9.9 x 10 ¹⁸	1.5 x 10 ¹⁷	-	-	.53	.31
NA21	SC18-5	4.9 x 10 ¹⁸	2 x 10 ¹⁷ (Te)	.45	6.35	-	-
	(Lo bump)						
NA21	SC19-3	8.5 x 10 ¹⁸	6.2 x 10 ¹⁷ (Te)	.45	6.35	.50	1.65
	(Lo bump)						
NA21	SC19-3	8.5 x 10 ¹⁸	6.2 x 10 ¹⁷ (Te)	.45	9.5	.50	2.44
	(Hi bump)						
NA21	SC20-3	7.0 x 10 ¹⁸	1.5 x 10 ¹⁸	.45	5.8	-	-
	(Hi bump)						
NA21	SC20-3	7.0 x 10 ¹⁸	1.5x10 ¹⁸ (Te)	.45	5.95	.50	.44
	(Hi bump)						
NA21	SC19-5	7.5 x 10 ¹⁸	3.8x10 ¹⁷ (Te)	.45	6.50	.50	1.30
	(Lo bump)						
NA21	SC19-5	7.5 x 10 ¹⁸	3.8x10 ¹⁷ (Te)	.45	4.66	-	-
	(Hi bump)						
NA21	SC21-3	1.3 x 10 ¹⁹	P-type	-	-	-	-

TABLE IX (Continued)
Spectral Response of Solar Cells Normalized Relative to Thermocouple

Diff. Run No.	Slice No.	P-Surface Conc/cm ³	Initial Base Conc (N) No/cm ³	$\lambda_3, (\mu)$	$I_3 (\mu a/\mu v)$	$\lambda_4 (\mu)$	$I_4 (\mu a/\mu v)$
NA16	SC13-6	1×10^{19}	1×10^{17}	.58	.014	.7(broad)	.0075
Mesa	SC13-6			.58	.255	.7(broad)	.262
NA16	SC14-2	4.2×10^{18}	1×10^{15}	-	-	.7	.000185
NA20	SC13-4	1.5×10^{19}	3.7×10^{16}	-	-	.73(broad)	.21
			(P-type)				
NA20	SC15-3	1.5×10^{19}	graded	-	-	-	-
NA20	SC17-3	9.9×10^{18}	1.5×10^{17}	-	-	.76(broad)	1.94
NA21	SC18-5	4.9×10^{18}	2×10^{17} (Te)	-	-	-	-
	(Lo bump)						
NA21	SC19-3	8.5×10^{18}	6.2×10^{17} (Te)	-	-	-	-
	(Lo bump)						
NA21	SC19-3	8.5×10^{18}	6.2×10^{17} (Te)	-	-	-	-
	(Hi bump)						
NA21	SC20-3	7.0×10^{18}	1.5×10^{18} (Te)	-	-	-	-
	(Lo bump)						
NA21	SC20-3	7.0×10^{18}	1.5×10^{18} (Te)	-	-	-	-
	(Hi bump)						
NA21	SC19-5	7.5×10^{18}	3.8×10^{17} (Te)	-	-	-	-
	(Lo bump)						
NA21	SC19-5	7.5×10^{18}	3.8×10^{17} (Te)	-	-	-	-
	(Hi bump)						
NA21	SC21-3	1.3×10^{19}	P-type	-	-	.78(broad)	11.7

TABLE X

Effect of Top Metal Contact to GaP Solar Cell on Open Circuit Voltage
GaP Solar Cell NA-16, SC14-2

Total Cell Area Uncovered <u>cm²</u>	Open Circuit Voltage <u>V_{oc} Volts</u>
. 22 (total cell area)	1. 05
. 16	1. 03
. 11	1. 00
. 077	. 98
0	0

TABLE XI

Diff. Run No.	Slice No.	V_{oc} (volts) at R. T.	J_{sc} (ma/cm ²) at R. T.	Max. J_{sc} (ma/cm ²)	t_m , °C	V_{ocm} Volts
NA-1	AP62-2	.60	.23	.40	250	0.20
NA-2	AP62-4	.55	.19	.42	325	.026
NA-8	bulk, poly	.060	.03	.07	225	.011
NA-10	"	.038	.10	.11	75	.027
NA-13	"	.080	.11	.12	125	.036
NA-16	SC14-2	1.08	.07	.24	400	.070
NA-16	SC13-6	.58	.01	3.7	300	.020
NA-20	SC13-4	.72	.13	.97	300	.034
NA-20	SC17-3	.60	.20	.63	250	.075
NA-20	SC15-3	.75	.012	.07	275	.018
NA-21	SC21-3	.72	4.35	4.6	200	.24
NA-22	SC13-6	.66	.007	1.17	300	.014
NA-21	SC19-5	.98	.18	.35	350	.23
NA-23	SC13-6	.72	.03	4.3	300	.050
NA-24	SC13-6	.52	.04	1.7	250	.055
NA-25	SC22-3	.92	.06	.22	400	.165
NA-25	SC23-3	1.08	.11	.53	450	.12
NA-25	SC24-3	1.12	.07	.24	375	.27
NA-25	SC24-5	1.12	.07	.21	325	.30
NA-25	SC25-3	.97	.28	.48	350	.12
NA-25	SC26-3	.92	.19	.88	250	.064
NA-21	SC20-3	1.00	.09	.34	375	.145

t_m (°C) = temperature (°C) where maximum short circuit current density occurs.

V_{ocm} = open circuit voltage at temperature where maximum short circuit current density occurs.

TABLE XII

Diffusion Run	Slice No.	J_{sc} ma/cm ²	Carrier Concentration after Diffusion	Diffusion Length, μ	C-V	I Layer (μ)	Gradient, a (No/cm ²)	n
NA-1	AP62-2	.23	1×10^{16}	.47	$1/c^2$	-	-	> 2
NA-20	SC17-3	.37	1×10^{15}	4.0 (?)	$1/c^3$	4.0	4×10^{19}	"
NA-20	SC15-3	.05	5×10^{16}	.27	$1/c^3$.27	2.4×10^{22}	"
NA-20	SC13-4	1	3×10^{17}	.18	$1/c^3$.17	1.5×10^{23}	"
NA-16	SC13-6	2	5×10^{18}	.045	$1/c^3$.015	1.9×10^{24}	"
NA-22	SC13-6	.056	5×10^{17}	.16	$1/c^3$.27	1.25×10^{23}	"
NA-23	SC13-6	.08	3×10^{16}	.88	-	.94	-	"
NA-24	SC13-6	.05	5×10^{14}	< 7.4 (?)	$1/c^3$	7.4	-	"
NA-21	SC21-3	3.5	5×10^{16}	< .0078	$1/c^3$	-	-	"
NA-21	SC19-5	.1	5×10^{14}	1	$1/c^3$	-	6.7×10^{18}	"

TABLE XIII
Effect of Junction Depth on J_{sc}

<u>Diff. Run No.</u>	<u>Slice No.</u>	<u>Junction Depth (μ)</u>	<u>V_{oc} (Volts)</u>	<u>J_{sc} (ma/cm^2)</u>
NA16	SC13-6	< 0.5	0.58	0.01
NA20	SC13-4	0.5	0.73	0.12
NA21	SC19-5	< 0.4	0.96	0.12
NA20	SC17-3	< 0.5	0.60	0.20
NA21	SC21-3	< 0.4	0.74	5.0
NA22	SC13-6	3	0.65	0.005
NA22	SC13-4	3	0.74	0.006
NA22	SC19-5	5	0.92	0.06
NA22	SC17-3	5	0.96	0.04
NA22	SC21-3	4	0.62	1.14

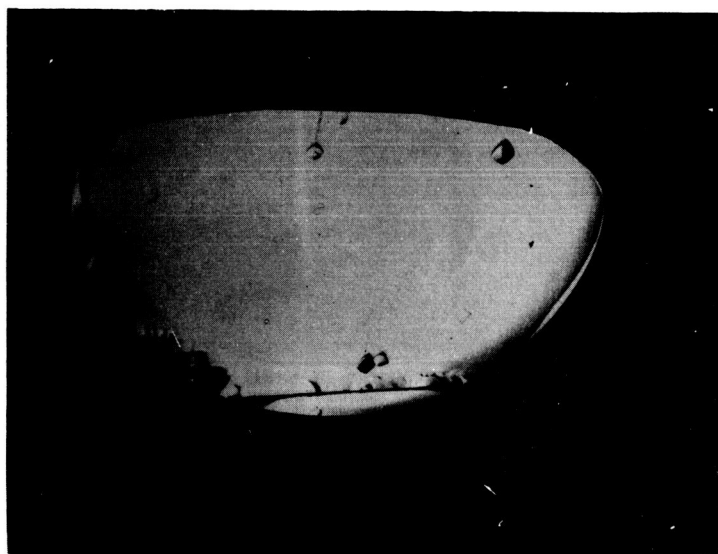


Fig. 1 - SC27-3, 25 μ . nearly bump free surface showing
effect of orientation

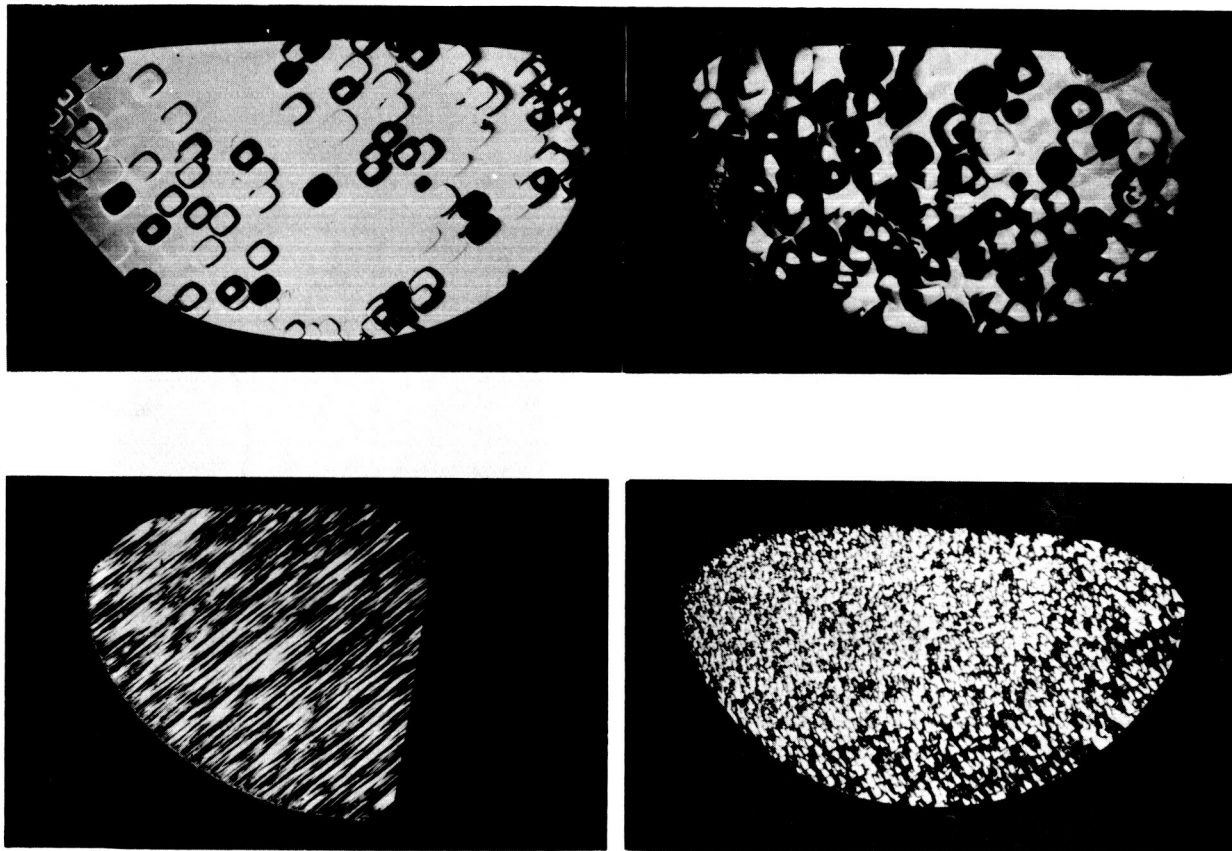


Fig. 2 - (a) SC18-5, $20\ \mu$, 2.0×10^{17} , "rounded rectangular" bumps, many with flat tops. (b) SC24-5, $57\ \mu$, 5.1×10^{17} , "square pyramidal" bumps. (c) SC16-3 $50\ \mu$, 1.9×10^{19} , parallel ridges caused by very heavy tellurium doping. (d) SC29-3, $55\ \mu$, 6×10^{18} (p), high concentration of bumps elongated in "A" direction caused by zinc doping.



Fig. 3 - (a) SC26-3, $45\ \mu$, $< 3.6 \times 10^{16}$, overlapping "square pyramidal bumps, 100x. (b) SC19-3, $34\ \mu$, 6.2×10^{17} , peaked rounded rectangular bumps, 100x. (c) SC29-3, $55\ \mu$, 6×10^{18} (p). Zn doped, well developed "p-type" elongated oval bumps, 200x. (d) SC30-3, $95\ \mu$, 3.2×10^{16} (n) Zn doped, small peaked "p-type" rounded rectangular bump, 100x.

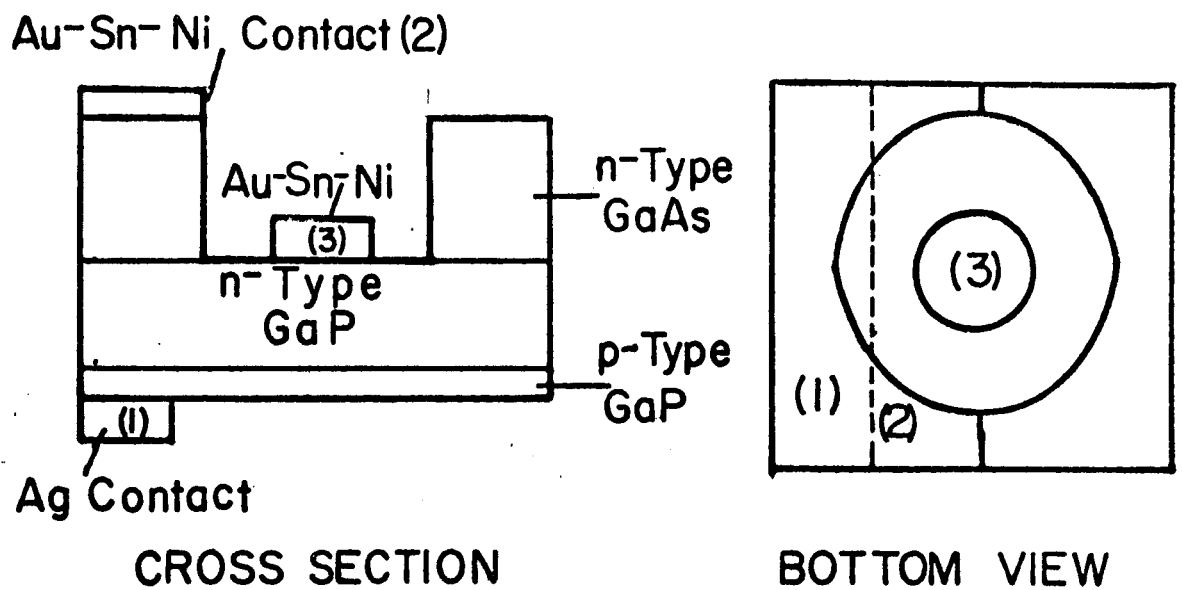


Fig. 4 - Experimental Set up for checking effect of GaP-GaAs interface.

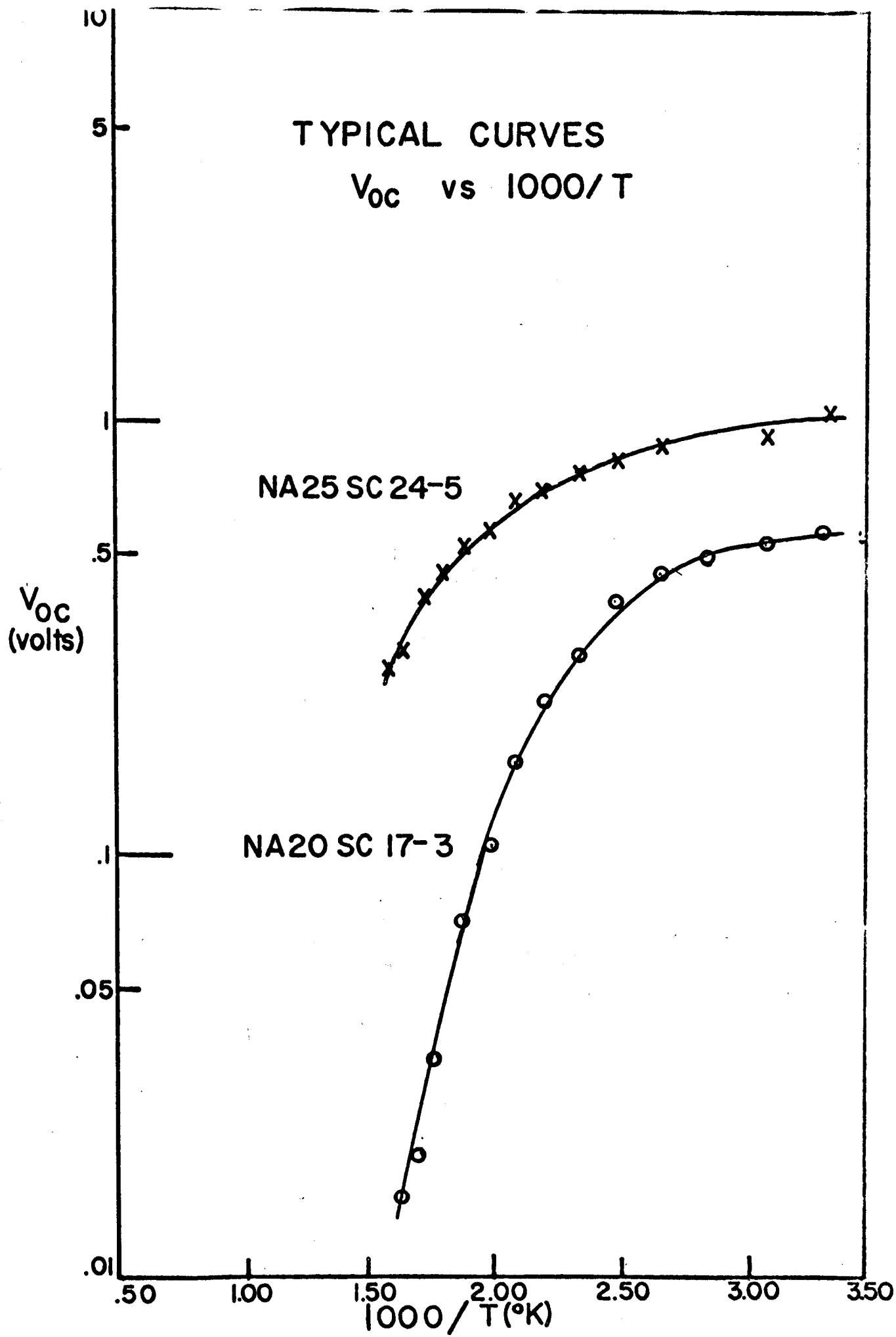


Figure 5

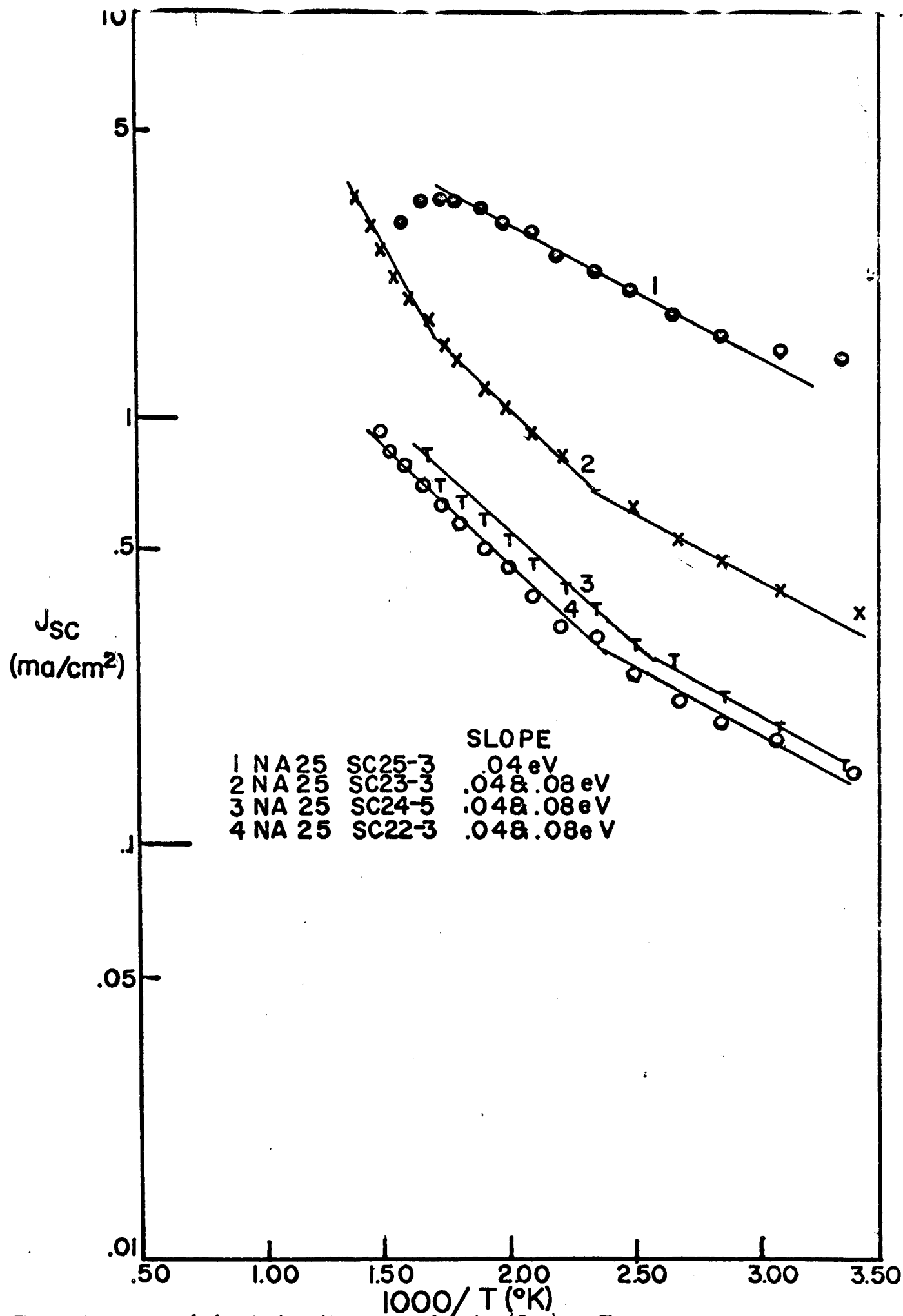


Fig. 6 - Typical curves of short circuit current density (J_{sc}) vs Temperature

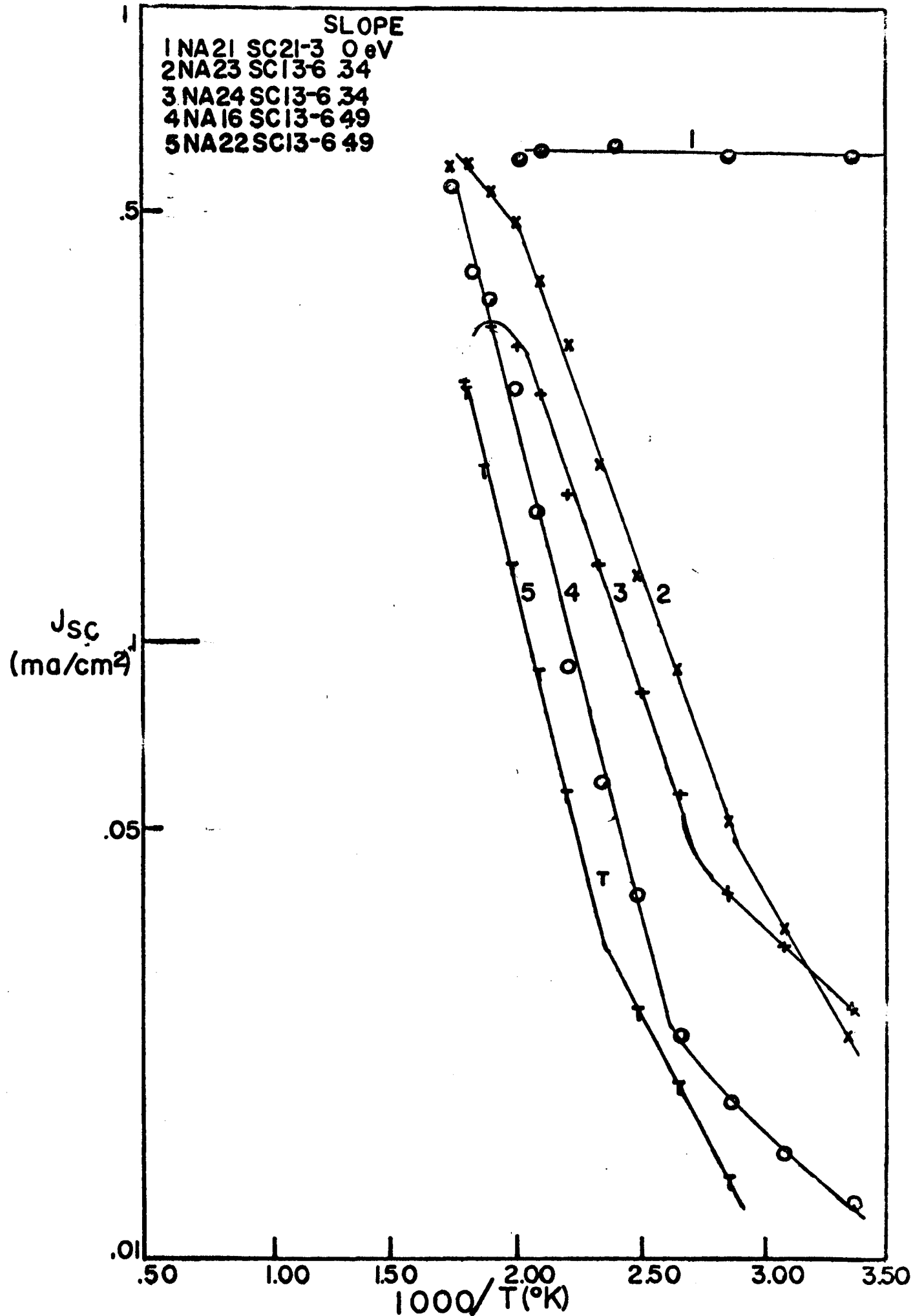


Fig 7 - Variation of short circuit current density (J_{sc}) with temperature

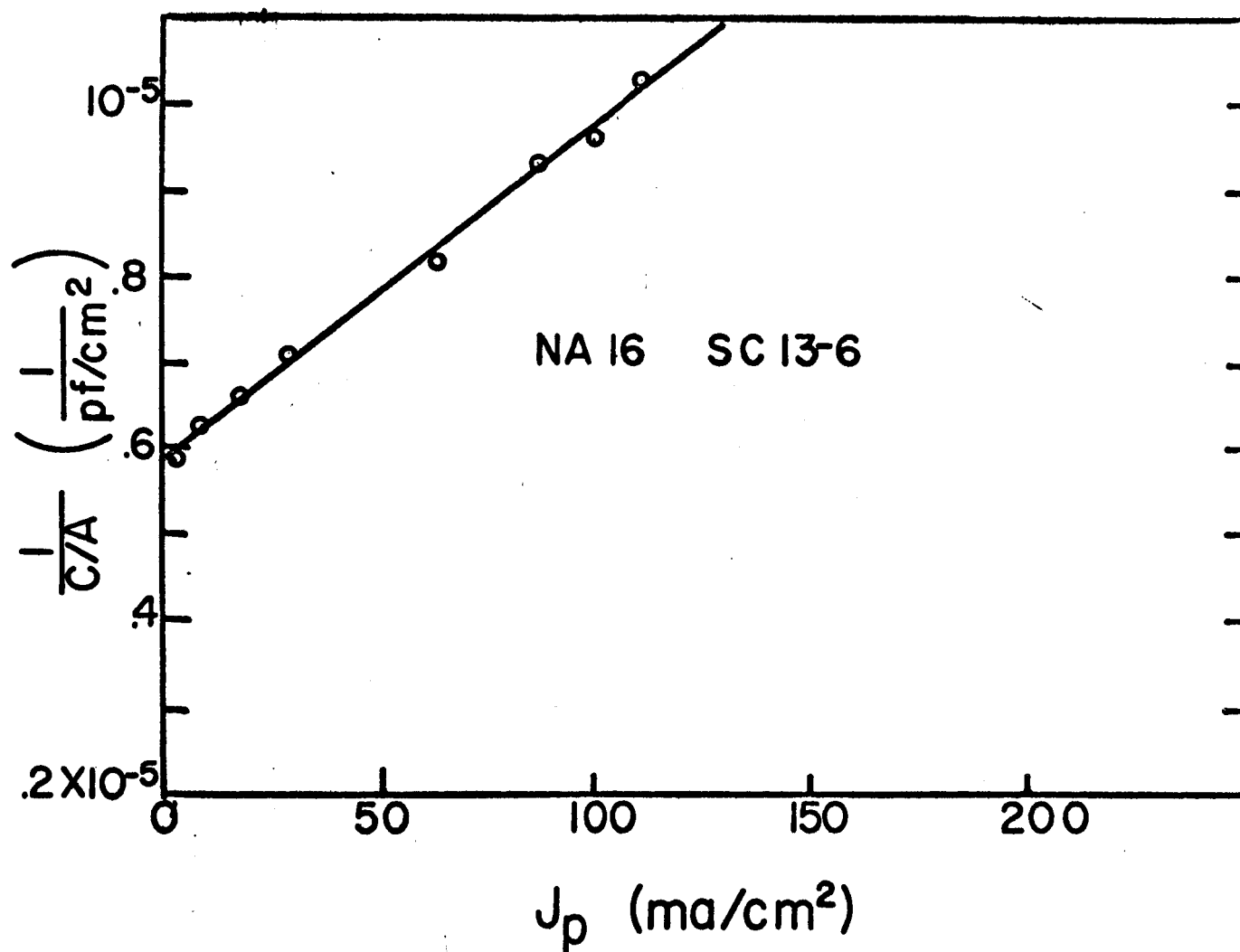


Fig. 8 - Sample plot used for determining minority carrier diffusion length.

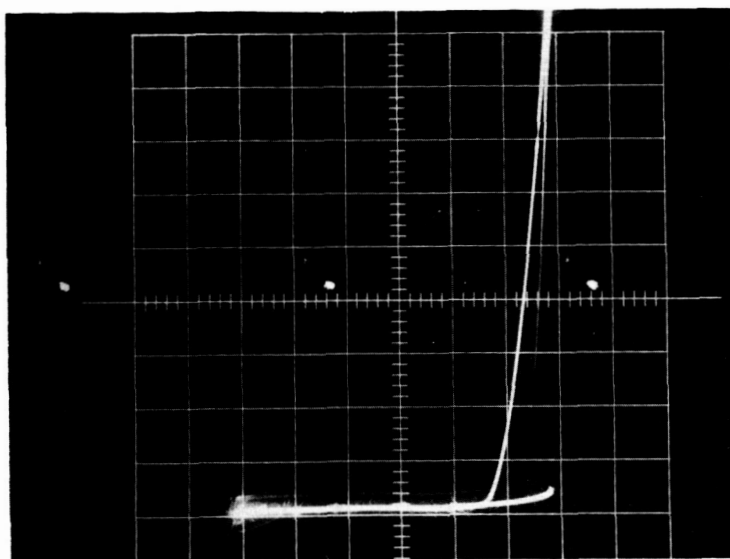


Fig. 9 - Negative resistance in forward direction for GaP mesa.
Sample NA24-SC13-6. Vertical: I , .2 ma/cm. Horizontal
Voltage, 1.25 volts/cm.

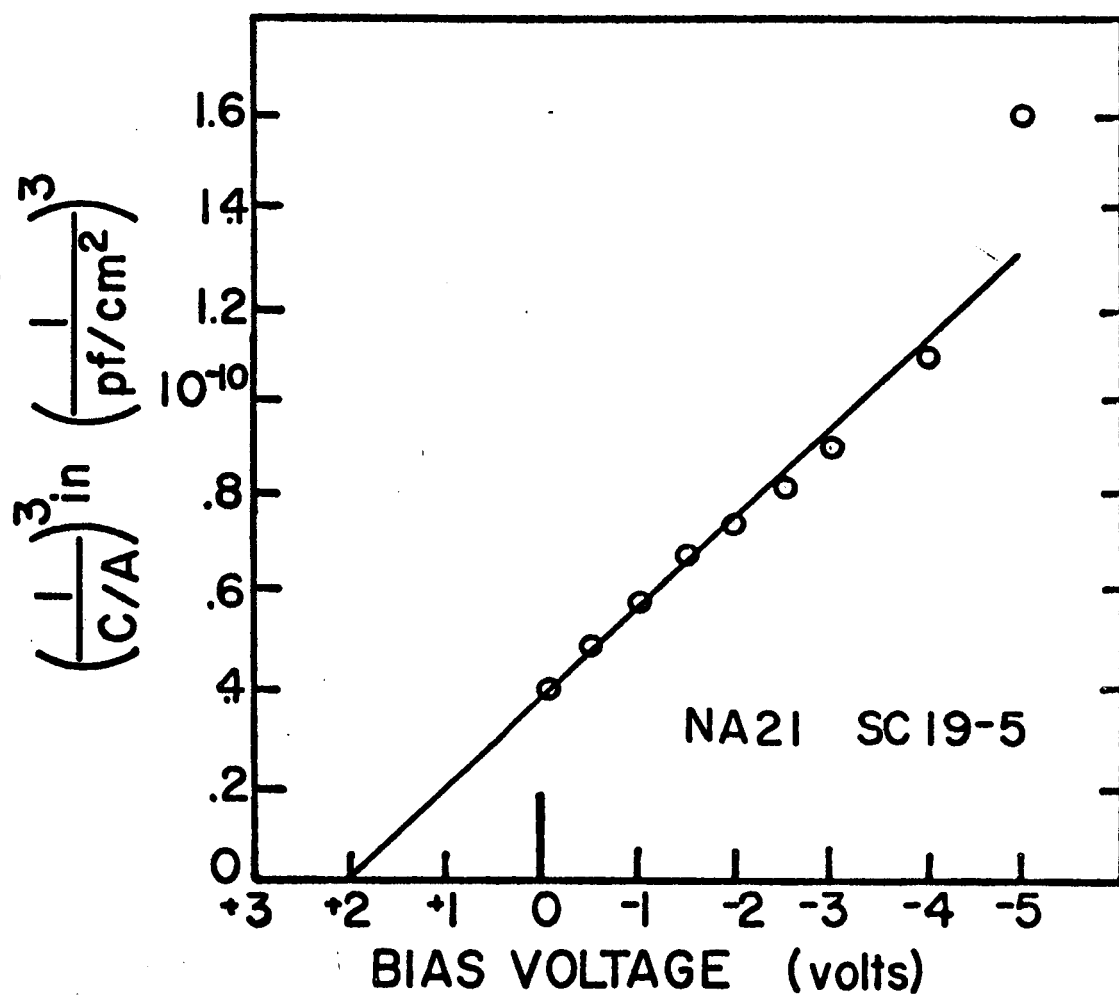


Fig. 10 - Plot of $1/c^3$ vs voltage for sample NA21 SC19-5

FRACTION of SOLAR ENERGY $> 2.2\text{ eV}$ ABSORBED

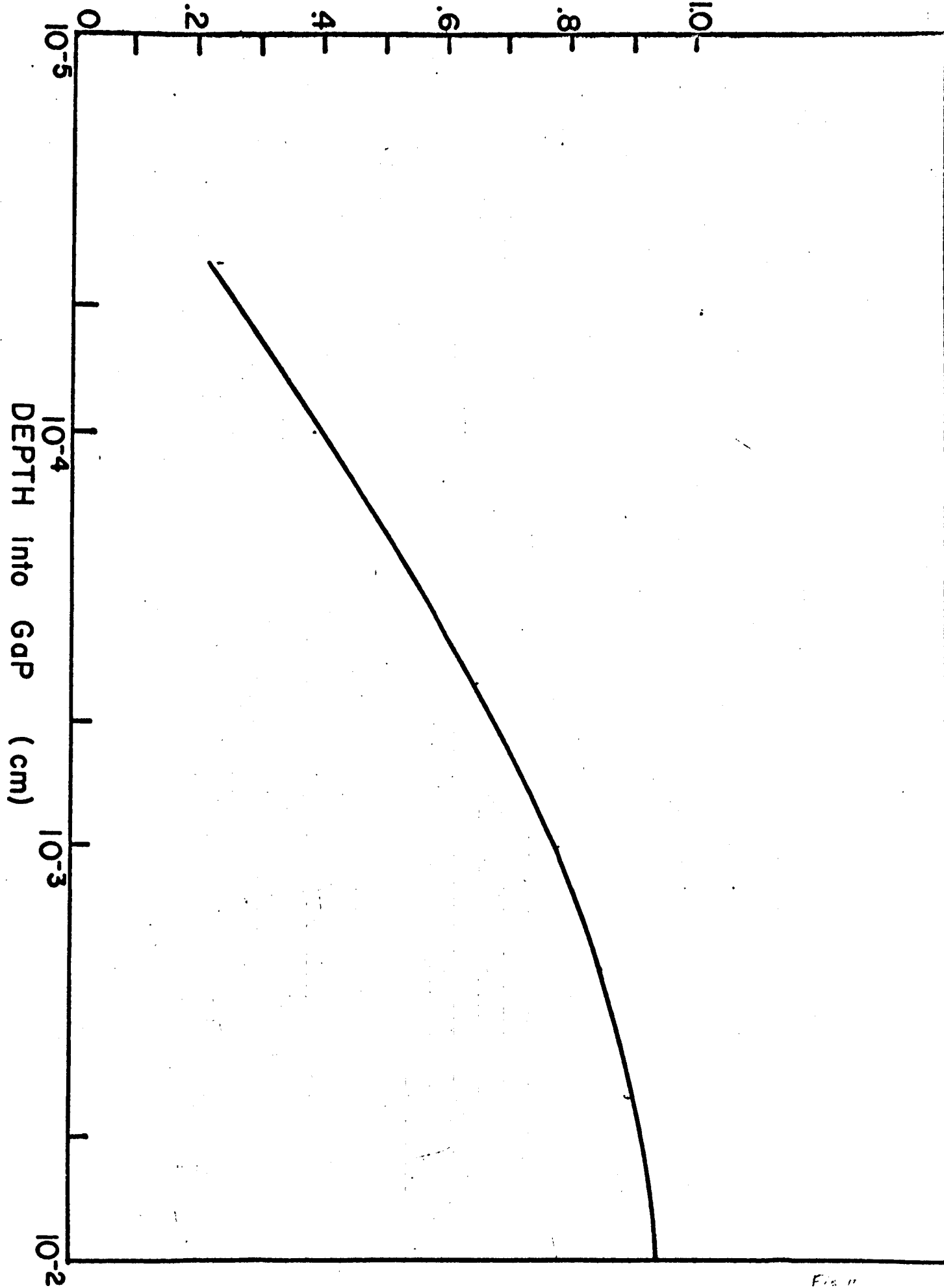


Fig. 11

DISTRIBUTION LIST

No. of Copies

National Aeronautics and Space Administration
Washington, D. C. 20546
Attn: Walter C. Scott/RP
J. L. Sloop/RP
Millie Ruda/AFSS-LD

1
1
1

National Aeronautics and Space Administration
Scientific and Technical Information Facility
Box 5700
Bethesda, Maryland 20546

3

National Aeronautics and Space Administration
Goddard Space Flight Center
Greenbelt, Maryland 20771
Attn: W. R. Cherry
M. Schach
B. Mermelstein, Code 672
J. W. Callaghan, Code 621
Librarian

1
1
1
1
1

National Aeronautics and Space Administration
Lewis Research Center
21000 Brookpark Road
Cleveland, Ohio 44135

Attn: J. J. Fackler, MS 86-1
B. Lubarsky, MS 86-1
H. Shumaker, MS 86-1
R. L. Cummings, MS 86-1
C. K. Swartz, MS 86-1
N. D. Sanders, MS 302-1
J. Broder, MS 302-1
J. Mandelkorn, MS 302-1
A. E. Potter, MS302-1
C. S. Corcoran, MS 100-1
N. T. Musial, MS 77-1
George Mandel, MS 5-5

1
1
1
1
4
1
1
1
1
1
1
1
1

National Aeronautics and Space Administration
Langley Research Center
Langley Station
Hampton, Virginia 23365
Attn: W. C. Hulton
E. Rind

1
1

DISTRIBUTION LIST

No. of Copies

Jet Propulsion Laboratory 4800 Oak Grove Drive Pasadena, California 91103 Attn: P. Goldsmith G. E. Sweetnam	1 1
Institute for Defense Analysis Connecticut Avenue, N. W. Washington, D. C. 20546 Attn: R. Hamilton	1
Advanced Research Projects Agency Department of Defense, Pentagon Washington, D. C. 20546 Attn: Dr. C. Yost	1
Naval Research Laboratory Department of the Navy Washington, D. C. 20546 Attn: E. Broncato, Code 6464 M. Wotaw, Code 5170 Dr. V. Linnenbom, Code 7450 Dr. C. Klick, Code 6440	1 1 1 1
U. S. Army Advent Management Agency Mission Equipment Department Ft. Monmouth, New Jersey Attn: William Scherr, SIGFM/PAM-5	1
U. S. Army Signal Research and Development Laboratory Fort Monmouth, New Jersey Attn: Power Sources Branch	1
Air Force Cambridge Research Center Air Research and Development Command USAF, Hanscom Field Bedford, Massachusetts Attn: Col. G. de Giacomo	1
Air Force Ballistic Missile Division Air Force Unit Post Office Los Angeles 45, California Attn: COL L. Norman, SSEM LT COL G. Austin, SSZAS CAPT A. Johnson, SSZDT CAPT W. Hoover, SSTRE LT COL A. Bush, SSZME	1 1 1 1 1

DISTRIBUTION LIST

No. of Copies

Wright Air Development Division Wright-Patterson Air Force Base Dayton, Ohio Attn: P. R. Betheand Mrs. E. Tarrants/WWRNEM-1	1 1
Flight Accessories Aeronautics Systems Division Wright-Patterson AFB Dayton, Ohio Attn: Joe Wise/ASRMFP-2	1
Aerospace Corporation P. O. Box 95085 Los Angeles 45, California Attn: Dr. G. Hove Dr. F. Mozer V. J. Porfune Dr. I. Spiro	1 1 1 1
Battelle Memorial Institute 505 King Avenue Columbus, Ohio Attn: L. W. Aukerman R. E. Bowman T. Shielladay	1 1 1
Bell and Howell Research Center 360 Sierre Madre Villa Pasadena, California Attn: Alan G. Richards	1
Bell Telephone Laboratories Murray Hill, New Jersey Attn: W. L. Brown U. B. Thomas	1 1
Clevite Research Center 540 E. 105th Street Cleveland Ohio 44108 Attn: Dr. Hans Jaffe	1
The Eagle-Picher Company Chemical and Material Division Miami Research Laboratories 200 Ninth Avenue, N. E. Miami, Oklahoma Attn: John R. Musgrave	1

DISTRIBUTION LIST

No. of Copies

Harshaw Chemical Company Solid-State Division 2240 Prospect Avenue Cleveland, Ohio 44115 Attn: James C. Schaefer	1
Heliotek Corporation 12500 Gladstone Avenue Sylmar, California Attn: Eugene Ralph	1
Hughes Aircraft Company Aerospace Group, R and D Division Culver City, California Attn: C. A. Escoffery	1
Leesona Moos Laboratories 90-28 Van Wyck Expressway Jamaica 18, New York Attn: Stanley Wallack	1
National Cash Register Company Physical Research Department Dayton 9, Ohio Attn: R. R. Chamberlin	1
North American Aviation, Inc. Autonetics Division Anaheim, California Attn: R. R. August	1
Philco Corporation Blue Bell, Pennsylvania Attn: Mr. A. E. Mace	1
Radio Corporation of America RCA Research Laboratories Princeton, New Jersey Attn: P. Rappaport	1
Radio Corporation of America Semiconductor and Materials Division Somerville, New Jersey Attn: Dr. F. L. Vogel	

DISTRIBUTION LIST

	<u>No. of Copies</u>
Sandia Corporation Albuquerque, New Mexico Attn: F. Smits	1
Solid-State Electronics Laboratory Stanford Electronics Laboratory Stanford University Stanford, California Attn: Prof. G. L. Pearson	1
Westinghouse Electric Corporation Research and Development Laboratories Churchill Borough, Pennsylvania Attn: H. C. Chang	1
Westinghouse Electric Corporation Semiconductor Division Youngwood, Pennsylvania Attn: Don Gunther	1